Geochimica et Cosmochimica Acta 378 (2024) 217–233

Contents lists available at ScienceDirect

Geochimica et Cosmochimica Acta

journal homepage: www.elsevier.com/locate/gca

Boron isotope pH calibration of a shallow dwelling benthic nummulitid foraminifera

Douglas Coenen [a,b,*], David Evans [a,b,1], Hagar Hauzer [c,d], Romi Nambiar [a,b], Hana Jurikova [e], Matthew Dumont [e], Puspita Kanna [f], James Rae [e], Jonathan Erez [c], Laura Cotton [g], Willem Renema [h,i], Wolfgang Müller [a,b]

[a] Institute of Geosciences, Goethe University Frankfurt, Frankfurt am Main, Germany
[b] Frankfurt Isotope and Element Research Center (FIERCE), Goethe University Frankfurt, Frankfurt am Main, Germany
[c] The Fredy and Nadine Hermann Institute of Earth Sciences, The Hebrew University of Jerusalem, Jerusalem, Israel
[d] Israel Oceanographic and Limnological Research, National Institute of Oceanography, Haifa, Israel
[e] School of Earth and Environmental Sciences, University of St Andrews, St Andrews, United Kingdom
[f] Marine Science Department, Hasanuddin University, Makassar, Indonesia
[g] Natural History Museum of Denmark, Copenhagen, Denmark
[h] Naturalis Biodiversity Center, Leiden, The Netherlands
[i] Institute of Biodiversity and Ecosystem Dynamics, University of Amsterdam, The Netherlands

ARTICLE INFO

Associate editor: Thomas M. Marchitto

Keywords:
Boron isotope
LA-MC-ICPMS
Foraminifera
pH proxy
Laboratory calibration
Symbiont-bearing

ABSTRACT

The boron isotope palaeo-pH/CO_2 proxy is one of the key quantitative tools available to reconstruct past changes in the concentration of CO_2 in the atmosphere. In particular, marine calcifying organisms have been shown to be useful archives of this proxy, enabling quantitative variations in pH/CO_2 to be reconstructed throughout the Cenozoic. In order to provide an alternative proxy archive to the widely used planktonic foraminifera, we investigated the symbiont-bearing, high-Mg, shallow-dwelling, tropical large benthic foraminifera (LBF) species *Operculina ammonoides* and present a calibration of the relationship between the shell boron isotopic composition and seawater pH. We investigated specimens collected from both several reefs as well as grown in laboratory culture experiments in which pH and DIC were decoupled from each other, measuring newly-formed chambers using laser-ablation as a sample introduction technique. Based on our laboratory culture samples, the resulting linear relationship between the *in situ* boron isotopic composition of aqueous borate ion ($B(OH)_4^-$) and the shells of *O. ammonoides* is characterised by a gradient of $0.38^{+0.12}_{-0.10}$. In contrast, the boron isotopic composition of the field collected samples displays a near 1:1 relationship with $B(OH)_4^-$. We suggest that the shallow slope of the laboratory culture regression is the result of the difference between their micro-environment carbonate chemistry and that of the surrounding seawater driven by a pH dependence of the relative rates of calcification and photosynthesis. Based on a model of the effect of these processes on the diffusive boundary layer, we show that this effect is expected in laboratory culture experiments free from micro-turbulence, but not in the foraminifer's natural environment. As such, we demonstrate the utility of these organisms as proxy archive, while also highlighting how laboratory experimental design has the potential to drive important changes in the micro-environment and resulting shell chemistry of organisms of this size. Given that the genus *Operculina* originated in the late Palaeocene, this work paves the way towards deep-time palaeo-pH/CO_2 reconstructions using foraminifer species which have a very closely related modern representative.

1. Introduction

Understanding the climate of Earth's geological past is key to characterising the broad features of warm climate states (Masson-Delmotte et al., 2021) and is also an important method of assessing state of the art model performance (e.g. Tierney et al., 2020). During the

* Corresponding author at: Institute of Geosciences, Goethe University Frankfurt, Frankfurt am Main, Germany.
E-mail address: coenen@geo.uni-frankfurt.de (D. Coenen).
[1] Present address: School of Ocean and Earth Science, University of Southampton, Southampton, United Kingdom.

https://doi.org/10.1016/j.gca.2024.06.020
Received 23 August 2023; Accepted 20 June 2024
Available online 23 June 2024

Cenozoic (66 Ma to present), the climate evolved from a hothouse, with global temperature ~15 °C higher than pre-industrial during the early Eocene (Inglis et al., 2020), to an ice-house world ultimately characterised by bipolar ice sheets in the past ~3.2 Myr (Zachos et al., 2008). This long-term change was punctuated by a number of climatic events, the study of which is key to understanding the complex relationship between climate, greenhouse gas concentrations, the biosphere, and surface processes (e. g. Westerhold et al., 2020). In addition, accurate and precise reconstructions of past changes in CO_2 are a prerequisite of constraining climate sensitivity from palaeo data (e.g. Anagnostou et al., 2016), with direct relevance to better understanding the likely magnitude of future global warming (PALAEOSENS, 2012). Within the scope of these broad aims, a key quantitative methodology for reconstructing CO_2 beyond the ice-core records is based on the boron isotopic composition of marine biogenic calcite (Sanyal et al., 1995; Hönisch et al., 2009; Rae, 2018; CenCO2PIP et al., 2023).

The boron isotope proxy is based upon the pH-dependent aqueous speciation of boron, with boric acid ($B(OH)_3$) and borate ion ($B(OH)_4^-$) dominating at low and high pH, respectively (Dickson, 1990). Being a light element, there is a large fractionation in the boron isotopic composition between these two species at low temperature, as they are characterised by a substantial difference in bond lengths between the B and OH group (Branson, 2018a). As a result, the boron isotopic composition of both species changes in tandem with their proportions in solution, which in-turn is dominantly driven by pH given that boric acid is weakly dissociative. If $B(OH)_4^-$ is the only, or dominant, species incorporated into $CaCO_3$, then the boron isotopic composition of the mineral should scale with the pH of the solution from which it was precipitated. In the case of marine calcifiers (especially foraminifera) it was initially hypothesised that only $B(OH)_4^-$ is incorporated into their calcite shell (Hemming and Hanson, 1992), as appears to be broadly the case for biogenic aragonite (Trotter et al., 2011; Anagnostou et al., 2012; McCulloch et al., 2017; Gagnon et al., 2021). However, many studies have since shown that there are significant kinetic and/or vital effects on boron incorporation into the shells of calcitic marine organisms (Zeebe et al., 2003; Hönisch et al., 2003; Foster, 2008; Rollion-Bard and Erez, 2010; Henehan et al., 2013, 2016). For these reasons, the application of the proxy to the fossil record generally requires the development of empirical calibrations, which account for the "vital effects" resulting from the biological process of calcification or kinetic processes involved in mineral growth (Sanyal et al., 1996; Henehan et al., 2013).

Here, we focus on *Operculina ammonoides*, a high-Mg calcite large benthic foraminifera (LBF) of the family Nummulitidae (Cotton et al., 2020). These foraminifera are symbiont bearing, shallow water tropical reef dwellers favouring oligotrophic conditions and a sandy substrate (Renema and Troelstra, 2001), that typically live at depths of 10–70 m (Hohenegger et al., 1999; Renema, 2002; Oron et al., 2018). These foraminifera do not yet have a boron isotope-pH calibration, and the advantages of working with these LBF are that i) their large size facilitates multiple geochemical measurements on the same individual specimens (e.g. $\delta^{11}B$ and major/trace element composition) and ii) the nummulitid foraminifera have a lineage extending back to the late Palaeocene, for example, the genus *Operculina* (or *Neoassilina*, see Holzmann et al., 2022) originated in the early Eocene (Hottinger, 1977). In addition, previous work has demonstrated that Eocene and modern representatives of this group are characterised by a similar shell (trace) element composition (Evans et al., 2013), suggesting that the biomineralisation strategy and related vital effects between the modern and fossil representatives of this family are very similar. As such, the calibration presented here is likely to be applicable to deep-time (Palaeogene) samples with a degree of confidence that may be difficult to obtain in some other foraminifera groups.

Here, we analysed *Operculina ammonoides* grown in a laboratory culture experiment in which aspects of seawater carbonate chemistry were varied independently of each other, i.e. varying DIC at constant pH, and vice versa. Samples of the same species were also collected from a number of reefs in the Indo-Pacific to compare boron incorporation in this species in its natural environment to the controlled laboratory setting.

We use laser ablation as a sampling technique coupled to a multi-collector inductively coupled plasma mass spectrometer (LA-MC-ICPMS) to generate a calibration of the relationship between the boron isotopic composition of foraminifera and seawater carbonate/boron chemistry. The relatively large test size of LBF (compared to planktonic or smaller benthic foraminifera) also makes these an ideal target for *in situ* elemental and isotopic measurements (Evans et al., 2015; Van Dijk et al., 2017).

2. Materials and methods

2.1. Laboratory culture experiments

Specimens of *Operculina ammonoides* were collected from the North Beach in the Gulf of Eilat in 2018. Bulk sediment containing abundant foraminifera was collected at a water depth of ~22 m, following which the bulk sample was transferred to the Institute of Earth Sciences at the Hebrew University of Jerusalem. Live foraminifera were identified as those that climbed on vertical glass slides placed in the sediments. Live foraminifera were sieved to retain specimens with uniform size (experiment HH6: 350–475 μm; HH7: 475–690 μm).

Before transfer to the experimental culture vessels, the foraminifera were placed in jars filled with seawater from the Gulf of Eilat with 40 μM calcein for five days (Erez, 2003; Evans et al., 2015; Hauzer et al., 2018). This membrane impermeable fluorescent dye enables chambers precipitated during the experimental period to be identified, as those grown in the jars before transfer to experimental seawaters will incorporate the dye, while the chambers grown during the experiment will not (Fig. 1a).

In addition, all culture seawaters were isotopically labelled with 74 nM ^{135}Ba (93%) to provide another means of unambiguously distinguishing newly precipitated chambers from those formed prior to collection (Evans et al., 2016). The low concentration of Ba in seawater (<10 μmol/mol) and the low natural abundance of ^{135}Ba (natural $^{135}Ba/^{138}Ba$ of 0.0919; Rosman and Taylor, 1997) enabled a small increase in the seawater [Ba^{2+}] to achieve an order of magnitude difference between the natural and experimental seawater $^{135}Ba/^{138}Ba$; the culture seawater was characterised by a $^{135}Ba/^{138}Ba$ of ~1. Because each experiment was spiked individually, there were small differences in the seawater $^{135}Ba/^{138}Ba$ between the experiments (between 0.7 and 1.2, see Figure S1). Once prepared, these seawater reservoirs were stored in airtight foil-lined inflatable bags to prevent re-equilibration of the carbonate system with the atmosphere.

The incubation of foraminifera was conducted in sealed glass jars containing 120 mL of experimental seawater. The cultured foraminifera experienced a 12 h dark-light cycles with an average of 40 μM photons/m^2/s from both natural and fluorescent light (Hauzer et al., 2021; typical variability of photon density within the laboratory can be seen in the supplementary materials of Evans et al. (2015)). The foraminifera were fed with 50 μL of frozen algae *Isochrysis,* diluted in seawater to ~0.1 g/L, after each water exchange (Hauzer et al., 2021).

Two main sets of experiments (HH6 and HH7) were conducted in which the concentration of dissolved inorganic carbon (DIC) and pH were decoupled from each other (Hauzer, 2022). To investigate the control of pH on the incorporation of boron and boron isotopes in *O. ammonoides,* in the first of these experiment sets (HH6) pH was varied at near constant DIC from ~7.4 to ~8.4 (Table 1) by changing the alkalinity of natural Gulf of Eilat seawater via HCl or NaOH addition (DIC = 2200 ± 119 μmol/kg_{sw}, 2SD of the experimental means). Salinity was unmodified at 40.65 on the practical scale. In addition, within the HH6 experimental set, two experiments were conducted at an elevated Ca^{2+} concentration ([Ca^{2+}_{SW}]; 13.7 and 17.7 mmol/kg_{sw} respectively) and lower than natural pH, to explore the potential influence of past changes

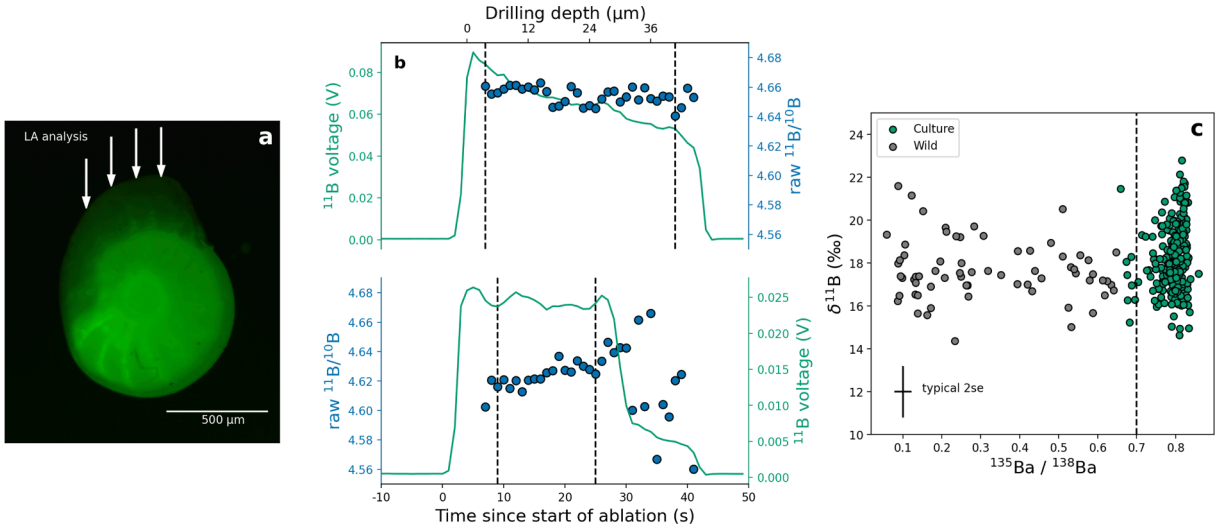

Fig. 1. Example boron and barium isotope analysis of cultured *Operculina ammonoides* using LA-MC-ICPMS. (a) Fluorescent microscope picture of a cultured *O. ammonoides* illustrating the use of calcein to identify chambers precipitated in the laboratory. The low fluorescence chambers (top) are those grown during the culture experiment. The direction of the laser ablation analyses is depicted by arrows. (b) Two examples of a time resolved laser ablation analysis. The dashed vertical black lines depict the locations at which the data was trimmed in the case of these specific samples. Both analyses were performed on cultured foraminifera using a laser spot size of 40 µm, a repetition rate of 6 Hz and a fluence of 6 J/cm^2. The analysis on top is an example of a stable signal with no chamber breakage whilst the bottom shows a chamber breakthrough after around 29 s of laser drilling. Drilling depth was estimated using an ablation rate of 200 nm/pulse at 6 Hz, 6 J/cm^2 (Griffiths et al., 2013). (c) Example use of ^{135}Ba/^{138}Ba to unambiguously identify material grown in laboratory culture, plotted against δ^{11}B at an adjacent locations in the shell (the Ba isotope analyses were laterally offset by ~ 20 µm from the boron isotope analyses, see text for details). The vertical dashed line delineates the cut-off point representing a value 10 % lower than the culture ^{135}Ba/^{138}Ba endmember. The green data points are those that are within uncertainty of the cut-off point, considered to have come from material grown under the experimental conditions.

Table 1
Measured and calculated chemistry of the culture jars for *Operculina ammonoides*. The jar pH and alkalinity were both measured, but the weighted pH and alkalinity were calculated (see text). Carbonate parameters were calculated using PyCO2SYS and the weighted pH and alkalinity used as inputs. The reported uncertainty for the saturation state of calcite ($\Omega_{calcite}$) is the median (50th percentile) with lower/upper percentiles corresponding to 2 SD. This was reported instead of a normal 2 SD because the resulting MC dataset is not normally distributed (see text).

Sample	Jar pH (NBS) Mean	Jar pH (NBS) 2 SD	Jar TAlk (µEq/kg) Mean	Jar TAlk (µEq/kg) 2 SD	pH_W (NBS) Mean	pH_W (NBS) 2 SE	$TAlk_W$ (µEq/kg) Mean	$TAlk_W$ (µEq/kg) 2 SE	DIC (µmol/kg) Mean	DIC (µmol/kg) 2 SD	$\Omega_{calcite}$ 2.5th	$\Omega_{calcite}$ 50th	$\Omega_{calcite}$ 97.5th
HH6-1	7.43	0.26	2205	21	7.49	0.15	1988	93	1964	104	0.83	1.14	1.56
HH6-2	7.66	0.19	2350	7	7.6	0.15	2034	118	1971	127	1.08	1.5	2.07
HH6-3	8.03	0.08	2495	14	7.89	0.24	2077	128	1903	160	1.70	2.75	4.29
HH6-4	8.37	0.31	2929	10	8.33	0.12	2333	172	1886	172	5.48	6.71	8.09
HH6-5	7.85	0.39	2507	22	7.74	0.16	2046	149	1937	156	1.68	2.34	3.22
HH6-6	7.51	0.38	2348	8	7.54	0.04	2006	165	1962	165	1.75	1.98	2.24
HH7-1	7.99	0.15	2832	12	7.95	0.12	2536	102	2334	115	2.76	3.51	4.42
HH7-2	7.73	0.61	938	50	7.91	0.07	832	27	731	26	0.98	1.02	1.07
HH7-3	7.84	0.38	1276	13	7.83	0.08	1130	41	1037	46	1.02	1.2	1.4
HH7-4	7.77	0.53	1580	408	7.77	0.03	1422	58	1334	57	1.27	1.37	1.48
HH7-5	7.99	0.34	2348	22	7.96	0.09	2084	78	1903	83	2.46	2.92	3.43
HH7-6	8.09	0.11	2264	5	7.93	0.18	2016	154	1850	164	1.84	2.65	3.74

in [Ca^{2+}_{SW}] on *O. ammonoides* δ^{11}B. Around 50 individuals of *O. ammonoides* were used per experiment. In contrast, the experiment set HH7 was designed to evaluate the possible control of seawater DIC on boron incorporation in *O. ammonoides* by keeping the pH constant ($pH_{NBS} = 7.90 \pm 0.28$, 2SD of the experimental means) and varying DIC concentration between 825 and 2460 µmol/kg$_{sw}$. The seawater used for HH7 was adjusted to a salinity of 37 by diluting seawater from the Gulf of Eilat with deionised water. For this set of experiments, around 80 individuals of *O. ammonoides* were placed into each culture.

The water in the experimental jars was exchanged every ten days with seawater from the reservoirs. Before the exchange, the pH and alkalinity of both the culture jars and reservoirs was measured and used to calculate the population growth rates of the foraminifera via alkalinity depletion (Segev and Erez, 2006; Oron et al., 2020) as well as to calculate the rest of the carbonate system (i.e. DIC, HCO_3^-, CO_3^{2-} concentrations and $\Omega_{calcite}$) using the Python version of CO2SYS (Lewis and Wallace, 1998; Humphreys et al., 2022). Details of the constants used to do so as well as error propagation are given in section 2.4. The culture jars were kept at a constant temperature of 25°C (±0.2 °C) by placing them into a water bath controlled by simultaneous cooling and heating (e.g. Evans et al., 2015). After 60 days, the experiment ended, and the foraminifera were rinsed with deionised water, after which they were dried and stored for later analysis. Before geochemical analysis, the samples were treated overnight with a dilute NaOCl solution (1.5 %) to remove organic material and rinsed several times with deionised water (Evans et al., 2015; Hauzer et al., 2021). Finally, a further series of ethanol and deionised water (18.2 MΩ cm) cleaning steps, 1x and 2x respectively, including 30 s ultrasonication were performed a few days before laser ablation analysis at the Frankfurt Isotope and Element Research Center (FIERCE) laboratories to remove any residual surface contaminations.

2.2. Laboratory culture carbonate chemistry calculations

While the carbonate chemistry conditions in both the culture jars and seawater reservoirs was highly controlled (Hauzer, 2022), some drift occurred in both cases because of calcification/photosynthesis/respiration of the foraminifera, and could be a result of a small amount of leakage or possible bacterial growth in the reservoirs. As such, the pH and DIC drifted by an average of 0.37 and 206 μmol/kg_{sw} respectively over the course of the experiment in the culture jars (see Table 1 and Fig. S2a). To account for this drift, bulk population growth rate curves were calculated using the alkalinity depletion method (e.g. Hauzer et al., 2018), following which, these curves were used to generate weighted averages of pH and DIC. This approach weights the average measurements towards the portions of the experiment in which the overall growth rate was highest, and assumes that portions of the experiment with greater bulk calcification rates are more likely to be included in our spatially-resolved measurements. Two other methodologies of average calculations, and the sensitivity of our results to them, are explored in the supplementary materials.

Previous work has demonstrated that, when culturing LBF, the resulting individual specimen calcification rates may vary greatly within the population (Hauzer et al., 2021). Some specimens may live longer than others, some may calcify mainly at the beginning of the experiment, while others may continue to calcify at a broadly constant rate irrespective of changes in the bulk population growth rate measured by alkalinity depletion. The question becomes: given a drift in pH and DIC with time, are the analysed chambers more likely to come from the part of the experiment when the overall population growth rate was higher? If so, a growth-rate weighted average might be more appropriate. Since we randomly selected specimens with at least one chamber precipitated in culture on the basis of calcein labelling, we consider it likely that we analysed foraminifera that stopped calcifying part-way through the experiment, such that average values of the seawater carbonate chemistry weighted to the population growth rates are likely to be the most appropriate characterisation of the conditions that the foraminifera experienced to relate seawater and shell geochemical data.

Specifically, we derived the fraction of the total growth that took place between each water exchange and used this to calculate weighted average and weighted standard error (following Gatz and Smith, 1995) of pH and total alkalinity (see Table 1). However, we note that none of our main conclusions are sensitive to this data treatment and all possible alternative averages of measured pH and total alkalinity used for the experiment are also explored in the supplementary materials.

2.3. Field-collected samples

As palaeoenvironmental reconstructions always use samples living and calcifying from naturally variable seawater, we additionally included field collected samples in an attempt to constrain the degree to which our culture experiments capture the salient features of the proxy and degree of unexplained variance in the calibration outside of a controlled environment (McClelland et al., 2021). Here, we analysed *Operculina ammonoides* or *Operculina* sp. samples collected from six different reefs in the Indo-Pacific, specifically the northernmost Red Sea, the Great Barrier Reef, and three reefs in Indonesia, namely the Spermonde archipelago, Kepulauan Seribu and Berau shelf (Table 3; see Evans et al., 2013; Renema, 2002, and references therein). Foraminifera were sampled and picked live from the sediments. Since the physical properties and chemical composition of the seawater were not measured at the time of collection (Renema, 2002; Renema et al., 2013), seawater measurements were taken from a mixture of literature values, monitoring stations and new *in-situ* measurements, discussed in more details in the supplementary materials. We also explored, in the supplementary materials, the use of a global seawater chemistry dataset (Gregor and Gruber, 2021) to compensate for the lack of direct seawater measurements for these sites, but find that it is not ideally suited to our purposes because of the regional-scale variability in seawater carbonate chemistry characteristic of shallow marine environments.

2.4. Carbon and boron system calculations

The carbonate system was determined from measured pH_{NBS} and total alkalinity using CO2SYS for the carbonate system calculations, including the concentration of calcium where this was experimentally modified (see below), silicate (0.3 μmol/kg_{sw}), and phosphate (0.05 μmol/kg_{sw}). The equilibrium constants K_1 and K_2 were taken from Lueker et al. (2000). These are recommended by Dickson (2007) and in addition, Raimondi et al. (2019) demonstrated the best internal consistency when reconstructing DIC from pH and total alkalinity when these constants are used.

Uncertainty was propagated via a Monte Carlo approach calling CO2SYS 10^5 times with random pH and total alkalinity values sampled from their uncertainty bounds (similar to Williams et al., 2017; Raimondi et al., 2019), assuming a normal distribution in both cases. The non-linear relationship between pH and other the carbon system parameters means that the resulting Monte Carlo dataset is not normally distributed when pH is the dominant source of uncertainty (Lauvset and Gruber, 2014; Orr et al., 2018). Each simulated parameter was individually screened by testing their normality with D'Agostino's K-squared test (D'Agostino and Pearson (1973); using the Python implementation in SciPy – Virtanen et al. (2020)). An example of parameter normality screening can be found in the supplementary materials (Figure S7). In the case of a normally distributed parameter, the median and 2 SD are reported, otherwise, the median, 2.5th and 97.5th percentiles are reported (Tables 1–3).

The values of pK_B* and $\delta^{11}B_{B(OH)4-}$ were calculated using the Python package *cbsyst* (Branson, 2018b) containing a fast implementation of MyAMI, which incorporates the pairing effects of Ca^{2+} and Mg^{2+} on the carbonate system equilibrium constants (Hain et al., 2015, 2018), and carbon/boron system simulation following CO2SYS. The use of MyAMI was especially relevant for the experiments HH6-5 and HH6-6 (Table 1) as they were both characterised by a higher Ca^{2+} concentration than natural seawater, which changed K_B* by ~1 and 3% respectively. We used a boron species fractionation factor (α_B) value of 1.027 ± 0.0006 (Klochko et al., 2006) and $\delta^{11}B$ of seawater = 39.61 ± 0.04 ‰ (Foster et al., 2010). Similarly to other carbon system parameters, 10^5 Monte Carlo simulations of the boron system were generated from pH data as well as temperature, salinity, $\delta^{11}B_{sw}$ and α_B.

To explore whether speciation controls the incorporation of boron in *Operculina ammonoides*, we used PHREEQC (Parkhurst and Appelo, 2013) to calculate the concentration of the $CaB(OH)_4^+$ and $MgB(OH)_4^+$ ion pairs in the experimental and natural seawaters, as well as activity coefficients of the carbonate and boron species. We used the pitzer database which is more suitable for application to solutions with higher ionic strength like seawater (I ≈ 0.7) (Farmer et al., 2019; Henehan et al., 2022; Nir et al., 2015). We followed the recommendations of Nir et al. (2015) and applied an offset of 0.19 to the pH total scale to compensate the MacInnes assumption used in PHREEQC, so the culture pH_{NBS} measurements were first converted to the total scale using CO2SYS from which the offset was then applied. The ionic composition of seawater was scaled with salinity (following Millero (2005) and Lee et al. (2010) for boron) except for calcium in the case that this was experimentally modified; in these cases the calculated total concentration was used. To calculate uncertainty of the simulations, a Monte Carlo approach was taken by performing 10^5 simulations with randomly sampled pH_{tot}, alkalinity, temperature, and salinity. The reported values are the median and 2.5th/97.5th percentiles. Similarly to Farmer et al. (2019), we observe an offset between pK_B* calculated using PHREEQC and CO2SYS/*cbsyst*, ranging from 0.088 to 0.093.

Table 2
The measured boron isotopic composition of cultured *Operculina ammonoides*. $\delta^{11}B_{B(OH)4-}$ was calculated using a Monte Carlo approach and used the weighted carbonate parameters as inputs (see text). The uncertainty of $\delta^{11}B_{B(OH)4-}$ is reported as percentiles of the 10^5 Monte Carlo simulated values.

Sample	pH_W (Total) Mean	pH_W (Total) 2 SE	$\delta^{11}B_{B(OH)4-}$ (‰) 50^{th}	$\delta^{11}B_{B(OH)4-}$ (‰) 2.5^{th}	$\delta^{11}B_{B(OH)4-}$ (‰) 97.5^{th}	$\delta^{11}B_{CaCO3}$ (‰) Mean	$\delta^{11}B_{CaCO3}$ (‰) 2 SE	B/Ca (mmol/mol) Mean	B/Ca (mmol/mol) 2 SE
HH6-1	7.35	0.15	13.63	13.19	14.2	16.09	0.62	0.21	0.03
HH6-2	7.47	0.15	14.08	13.51	14.85	16.86	0.38	0.26	0.02
HH6-3	7.76	0.24	15.73	14.32	17.85	17.56	0.48	0.36	0.03
HH6-4	8.2	0.12	20.22	18.8	21.8	19.45	0.34	0.45	0.03
HH6-5	7.61	0.16	14.77	14	15.8	17.71	0.23	0.33	0.02
HH6-6	7.41	0.04	13.89	13.72	14.07	17.41	0.41	0.31	0.03
HH7-1	7.81	0.12	15.98	15.14	16.99	17.55	0.25	0.28	0.02
HH7-2	7.78	0.01	15.73	15.63	15.82	18.07	0.26	0.36	0.02
HH7-3	7.69	0.08	15.14	14.68	15.67	17.75	0.21	0.31	0.02
HH7-4	7.64	0.03	14.81	14.64	14.99	17.32	0.24	0.28	0.02
HH7-5	7.82	0.08	16.05	15.43	16.75	17.19	0.27	0.28	0.01
HH7-6	7.79	0.18	15.81	14.67	17.36	17.85	0.38	0.32	0.02

2.5. Boron isotope and B/Ca analytical details

2.5.1. Laser-ablation MC-ICPMS boron isotope analytical methodology

All boron isotopic measurements were performed using the LA-MC-ICPMS setup at the Frankfurt Isotope and Element Research Center (FIERCE) at Goethe University Frankfurt, following the methodology outlined in Evans et al. (2021). This consists of a RESOlution M−50 LR 193nm ArF laser ablation system (Applied Spectra, formely Resonetics; Müller et al. (2009)) connected to a Neptune plus MC-ICPMS (ThermoFisher Scientific). The RESOlution LR is equipped with the large two-volume Laurin Technic S-155 ablation cell. He was used as the main cell gas, with the Ar sample gas from the ICPMS admixed into the top of the inner cell funnel. N_2 was added downstream of the ablation cell to improve sensitivity (Lin et al., 2014), see Table S1 for details. Nylon-6 tubing was used throughout (Evans and Müller, 2018).

To distinguish between the chambers grown under the experimental conditions (in ^{135}Ba-enriched seawater) from those already present, the $^{135}Ba/^{138}Ba$ of the foraminifera marginal cord was measured prior to the boron isotopic measurements. While the barium isotope ratio would ideally have been measured at an identical location as the boron isotopic measurement, this would not have been possible without either peak hopping or loss of material caused by ablating the same location more than once. Instead, $^{135}Ba/^{138}Ba$ measurements were made as close as possible to the $\delta^{11}B$ measurements with a smaller laser beam.

For the boron isotopic measurements, the faraday cups were arranged to simultaneously measure ^{10}B (L3) and ^{11}B (H4) as well as to monitor the Ca interference that is present across the mass range 10–11 on the Neptune (Sadekov et al., 2019; Standish et al., 2019; Evans et al., 2021). Specifically, we measured the elevated baseline that results from the ablation of Ca-rich materials at m/z 10.035 (L2, cf. 10.089 in Evans et al., 2021) and 9.979 (L4), although we ultimately only use the former in correcting the measurements. All the measurements were performed at low mass resolution, with 10^{13} Ω resistors installed on all four cups.

All gas flows and mass spectrometer parameters were optimised daily, see Table S1 for more details. Tuning was carried out by ablating NIST SRM612 with a 90 µm spot at 6 Hz repetition rate and ~6 J/cm^2 fluence to achieve a sensitivity between 3–4 V/mg/g and a background measurement on ^{11}B between 0.5 and 1 mV.

Instrumental mass bias was corrected using sample-standard bracketing with NIST SRM612 as the primary standard. The matrix interference present on ^{10}B when ablating samples with a Ca matrix on the Neptune plus was corrected by determining the relationship between the inaccuracy in the NIST SRM612-standardised $\delta^{11}B$ (the difference between measured $\delta^{11}B$ and accepted $\delta^{11}B$ value) and $^{11}B/10.035$ (proportional to B/Ca) for three well characterised carbonate standards, and applying this relationship to all samples (Standish et al., 2019; Evans et al., 2021). The three pressed powder pellet carbonate reference materials used here were: JCt-1 (*Tridacna gigas*) and JCp-1 (*Porites* sp.), both prepared by Dr Edmund Hathorne (GEOMAR) with $\delta^{11}B$ equal to 16.39 ± 0.60 ‰ and 24.36 ± 0.45 ‰ respectively (2SD of interlaboratory means, Gutjahr et al. (2020)), and MACS-3 (USGS synthetic calcite) with a $\delta^{11}B$ value of −0.57 ± 0.11 ‰ (2SD of three solution measurements; Standish et al. (2019)). The secondary standards were randomly distributed throughout the analysis sequence and analysed in an identical way to the samples, with at least 15 of each within a typical 12-hour session. All boron isotope analysis were carried out with a ~1.049 s integration time for 40 s drilling/spot analysis, with all samples and standard measurements bracketed by 20 s of gas blank analysis.

Reproducibility and accuracy were assessed using three secondary standards: the UWC-1 and UWC-3 marble standards, initially developed for SIMS oxygen isotope analysis (Edwards and Valley, 1998; Graham et al., 1998) and an in-house calcite standard (DE-B) which is a inorganic blue calcite acquired from an mineral dealership. The boron isotopic composition of UWC-1 was characterised by Standish et al. (2019); $\delta^{11}B$ = 7.77 ± 0.89 ‰. However, to our knowledge, no solution-based measurement is available for UWC-3 and our in-house standard DE-B had not previously been assessed. To address this, and report accuracy and precision across more than one standard not utilised in our data processing, we determined the composition of both materials independently of our laser-ablation methodology using solution-MC-ICPMS (see Sec. 2.5.2). DE-B is characterised by an average value of −0.02±0.41 ‰ (n = 20), while UWC-3 $\delta^{11}B$ = 20.25±0.08 ‰ (2σ, n = 2).

When comparing the intermediate precision (2SD variance in inter-session mean measured values within one laboratory) of measured $\delta^{11}B$ from the three external calcite standards (UWC-1, UWC-3, DE-B) from 41 laser ablation sessions (days) with solution-MC-ICPMS measurements, we observe a 1:1 relationship (Fig. S8), with an average overall difference of 0.89±0.38 ‰ (2SD). The individual intermediate precision difference between laser ablation and solution derived values are as follows: UWC-1: +0.86±0.31 ‰ (2SE), UWC-3: +0.72±0.27 ‰ and DE-B: +1.09±0.16 ‰. Given that the majority of these measurements are within the combined uncertainty of the two techniques, we do not apply an accuracy correction to the laser ablation data.

Given the fragility of the cultured *Operculina ammonoides* samples, specimens were mounted vertically to ablate the marginal cord (Fig. 1a) by carefully placing them onto a pressure sensitive adhesive. The marginal cord of the cultured samples was thin (<50 µm), so a 40×40 µm square spot size was the largest that could be used.

Following the data processing procedure described above and in detail in Evans et al. (2021), each analysis was individually screened to discard erroneous measurements or those in which the marginal cord was almost immediately broken, using the ^{11}B voltage and raw $^{11}B/^{10}B$, as well as images from the laser ablation camera system collected during analysis (Fig. 1b).

Table 3
Details of the field collected *Operculina ammonoides*. Alkalinity (TAlk), pH and temperature (T) were taken from a mixture of literature values, monitoring stations and *in situ* measurements, see text and supplementary materials. $\delta^{11}B_{B(OH)4-}$ was calculated from the aforementioned parameters using a Monte Carlo approach (see text). GBR stands for Great Barrier Reef.

Sample	Location	Lat (decimal degrees)	Long (decimal degrees)	pH (total) mean	pH (total) 2 SD	TAlk (μmol/kg) Mean	TAlk (μmol/kg) 2 SD	T (°C) Mean	T (°C) 2 SD	$\delta^{11}B_{B(OH)}$ 4- (‰) 50th	$\delta^{11}B_{B(OH)}$ 4- (‰) 2.5th	$\delta^{11}B_{B(OH)}$ 4- (‰) 97.5th	$\delta^{11}B_{CaCO3}$ (‰) Mean	$\delta^{11}B_{CaCO3}$ (‰) 2 SE	B/Ca (mmol/mol) Mean	B/Ca (mmol/mol) 2 SE
PD28	Makassar	−5.06	119.42	7.91[a]	0.16	2208	45	28[b]	0.4[b]	16.96	15.57	18.64	18.01	0.28	0.25	0.02
SSO7G14	GBR	−19.73	150.12	8.06	0.04	2285	20	26.6[b]	3.5[b]	18.31	17.71	18.91	18.55	0.2	0.39	0.02
SER33	Jakarta	−5.86	106.64	7.83[a]	0.09	1920[c]	200[c]	29[b]	0.5[b]	16.3	15.44	17.22	16.09	0.32	0.39	0.02
Eil19	Gulf of Eilat	29.54	34.97	8.06[d]	0.03[d]	2505[d]	16[d]	24[d]	4[d]	18.45	17.69	19.21	18.03	0.28	0.32	0.02
BBX49a	Celebes Sea	1.39	118.82	7.9[a]	0.02[†]	2213	53	29.2[b]	0.9[b]	16.84	16.31	17.36	17.03	0.41	0.33	0.03
KKE30	Makassar	−5.11	119.29	7.91[†]	0.16	2205	66	28[b]	0.4[b]	16.95	15.57	18.62	16.84	0.22	0.27	0.01

[a] pH measurement from nearby reefs.
[b] Temperature taken from Evans et al. (2013).
[c] Measurement from Afdal et al. (2024).
[d] Measurement from monitoring station of InterUniversity institute of Marine Sciences in Eilat.

2.5.2. Solution-MC-ICPMS analytical methodology

Solution MC-ICPMS analysis of the two standards without previous measurements was carried out in the St Andrews Isotope Geochemistry laboratories (STAiG) of the University of St Andrews, UK. Several grains of DE-B, separated from two different crushed hand samples (DE-B1 and DE-B2), and two grains of UWC-3 were selected and powdered to give ~1–2 mg aliquots for boron isotope analysis. Unlike laser ablation analysis, it is common practice to perform chemical pre-cleaning of samples prior to solution analysis. The possible impact of this pre-cleaning on the boron isotopic composition of these inorganic calcites was tested by further splitting each sample into two halve and performing the pre-cleaning step on one of them. The first halves of each aliquot went through a full cleaning procedure designed for biogenic carbonates from sediments involving clay removal rinses with boron-free deionised water (18.2 MΩ cm) and an oxidative cleaning step using 1 % H_2O_2 buffered with 0.1 M NH_4OH at 80 °C, before dissolution in 0.5 M HNO_3 (e.g. Barker et al. (2003); Jurikova et al. (2019)). The second half was rinsed twice with boron-free deionised water (18.2 MΩ cm) and dissolved with the aid of ultrasonication in 0.5 M HNO_3.

Prior to boron isotope analyses, boron was purified from the $CaCO_3$ matrix using boron-specific anion exchange resin, Amberlite IRA 743, crushed and sieved to 63–106 μm. Dissolved DE-B and UWC-3 aliquots were processed alongside RM NIST 8301 Foram (Stewart et al., 2021) and total procedural blanks (TPBs). Purified boron solutions were spiked with HF to aid boron wash out and measured in an 0.5 M HNO_3 plus 0.3 M HF matrix (Zeebe and Rae, 2020) on a Thermo Scientific Neptune Plus MC-ICPMS equipped with a HF-resistant sample introduction kit and 10^{13} Ω resistors. Instrumental mass bias was corrected by standard sample-bracketing with a 10 μg/g NIST SRM 951 solution. The average $\delta^{11}B$ for RM NIST 8301 Foram was 14.61 ± 0.19 ‰ (2SD, n = 4) and the TPBs were <7 pg B, negligible against the typical sample size of ~ 5 ng B.

No significant difference between uncleaned and cleaned values were observed for DE-B with average $\delta^{11}B$ values of −0.18 ± 0.32 ‰ (2SD, n = 10) for DE-B1 and 0.14 ± 0.19 ‰ (2SD, n = 10) for DE-B2, such that an overall average value of −0.02 ± 0.41 ‰ was used for the DE-B calcite in-house standard when comparing to LA-MC-ICPMS data. In addition, pieces of the MACS-3 pressed pellet used in the FIERCE laboratory were also measured after the aforementioned treatment. The resulting solution measured value is −1.22 ± 0.20 ‰ (2σ).

2.5.3. LA-MC-ICPMS barium isotope analytical methodology

The $^{135}Ba/^{138}Ba$ composition of the cultured foraminifera was measured close to the ablation pits of the $\delta^{11}B$ measurements as described above. The Faraday cups were arranged to simultaneously measure ^{135}Ba (L2) and ^{138}Ba (H2). The large difference in $^{135}Ba/^{138}Ba$ (~10 times higher) between culture and non-culture material in the experiments reported here allowed for a smaller spot size of 15×15 μm and shorter analysis (5 s). No mass bias correction or standardisation was applied to the data, because we are here interested in order-of-magnitude-scale changes in the barium isotopic composition of the shells. Nonetheless, repeat analysis of the JCp (pressed pellet) reference material measured under the same conditions yielded a measured $^{135}Ba/^{138}Ba = 0.0899 + 0.0120$ (2SD), such that these non-standardised measurements are demonstrably sufficiently accurate and precise to determine the large variability in isotopic composition characteristic of the samples studied here. The same repetition rate (6 Hz) and fluence (6 J/cm^2) as for the $\delta^{11}B$ measurements were used. The resulting $^{135}Ba/^{138}Ba$ were matched to the closest boron isotope ablation pit in order to determine which boron isotope measurements should retained or discarded based on their artificially-high or natural $^{135}Ba/^{138}Ba$ ratio.

2.5.4. LA-SF-ICPMS B/Ca determination

To determine whether B/Ca can be accurately characterised using the $^{11}B/10.035$ ratio obtained during the isotopic analysis, trace element analysis for B/Ca measurements was performed on the same samples

using a Thermo-Scientific Element XR SF-ICPMS in the FIERCE laboratories, connected to the same laser ablation system (see Table S2). Tuning was performed daily by ablating NIST SRM612 with a 60 µm laser beam and 6 Hz repetition rate, with a typical sensitivity of >6x10^6 cps of ^{238}U under these conditions, while maintaining $ThO^+/Th^+ < 1$ %, U/Th = 0.94 – 0.97 and *m/z* 44/22 < 2 % (to monitor doubly-charged ion production). The marginal cord of the samples was ablated using a 50 µm spot and a repetition rate of 3 Hz, with the "squid" signal smoothing device added downstream of the ablation cell to obtain a stable signal (Müller et al., 2009). B/Ca ratios were quantified using standard procedures (Heinrich et al., 2003), with ^{43}Ca as an internal standard and NIST SRM610 as the external calibration standard (using the NIST SRM610 [B] value of Jochum et al. (2011)). Data reduction was performed using an in-house Matlab script (Evans and Müller, 2018), with the details of trace element data reduction described elsewhere (Evans et al., 2015; Nambiar et al., 2023). Accuracy of three secondary standards, namely GOR-128G, JCt-1 and MACS-3 (Jochum et al., 2005, 2019; Hathorne et al., 2013) was ~4%, ~3% and ~2% respectively.

3. Results

3.1. Boron isotope calibration

All results are displayed in Figs. 2-4 and Tables 1-3. The measured boron isotopic composition of the cultured *Operculina ammonoides* ranges between 16.1 ‰ (HH6-1, lowest pH experiment) and 19.5 ‰ (HH6-4, highest pH experiment) (Table 2). Most of the samples have a boron isotope value heavier than the boron isotopic composition of *in situ* $B(OH)_4^-$, with a greater offset at lower pH.

The resulting boron isotope calibration of the cultured samples is plotted in Fig. 2 as a regression between measured $\delta^{11}B_{CaCO3}$ and calculated $\delta^{11}B_{B(OH)4-}$, based on the physical and chemical properties of the water in which the foraminifera grew (Section 2.4). Once a relationship between measured $\delta^{11}B_{CaCO3}$ and calculated *in situ* $\delta^{11}B_{B(OH)4-}$ is derived, it allows for the conversion of future measurements into estimates of *in situ* $\delta^{11}B_{B(OH)4-}$ which in turn can be used to estimate the *in situ* pH (Foster et al., 2012).

As a result of non-linearities in the carbonate system (Section 2.4), the calculated $\delta^{11}B_{B(OH)4-}$ values of all experimental seawaters are not normally distributed. As such, we determine the best-fit linear regression through the data using a Monte Carlo approach by performing linear regressions through 10^5 randomly generated $\delta^{11}B_{CaCO3}$ (within their uncertainty bounds) and $\delta^{11}B_{B(OH)4-}$, the latter derived as reported above. Since the uncertainties in $\delta^{11}B_{B(OH)4-}$ are not normally distributed, neither are the resulting gradients and intercepts such that we report the median and 2.5th and 97.5th percentiles (Eq. (1).

$$\delta^{11}B_{B(OH)_4^-} = \frac{\delta^{11}B_{CaCO_3} - \left(11.71^{+1.47}_{-1.88}\right)}{0.38^{+0.12}_{-0.10}} \quad (1)$$

Based on a simple least-square regression (OLS), the goodness of fit statistics are as follows: $R^2 = 0.76$, Root Mean Square Error (RMSE) is 0.37 ‰ and p=0.0002. With a gradient lower than one (0.38) in borate space, the boron isotopic calibration of cultured *O. ammonoides* appears to be buffered against external pH, given that this is the only major control on $\delta^{11}B_{B(OH)4-}$ in these experiments. The alternative seawater carbonate chemistry calculation discussed in section 2.2, yield similar gradient and intercept values, albeit with a reduced goodness of fit (Fig. S3). The weighted pH of the experimental jars is also a good predictor of $\delta^{11}B_{CaCO3}$ in our experiments (Fig. 2b), with a non-linear logistic fit yielding the following statistics: $R^2 = 0.75$, RMSE = 0.38 ‰ and $p = 0.002$. While we do find a negative relationship between DIC and

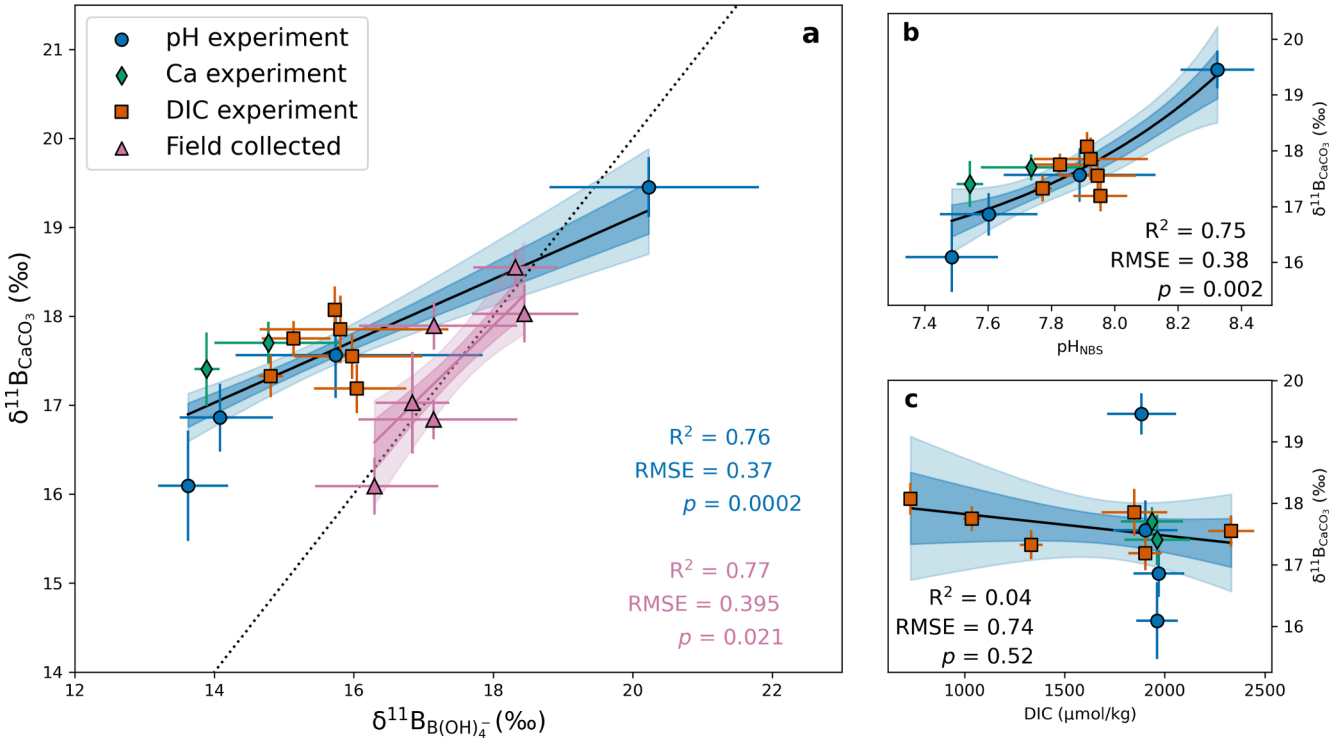

Fig. 2. Boron isotope calibration of *Operculina ammonoides*. (a) Regression between the measured $\delta^{11}B_{CaCO3}$ and calculated *in situ* $\delta^{11}B_{B(OH)4-}$. Uncertainties are 2 SE in the case of $\delta^{11}B_{CaCO3}$ and 2.5th and 97.5th percentiles of the Monte Carlo derived $\delta^{11}B_{B(OH)4-}$ (see text for details). The linear regression through the culture data was performed using a Monte Carlo approach by fitting a line through data points randomly sampled from their uncertainty boundaries 10^5 times (blue regression). The statistics for this regression are displayed in blue in the bottom right corner. The pink regression, similarly calculated as above, is fitted through the field collected samples. The statistics for this regression are displayed in pink in the bottom right corner. The displayed confidence region of the regression is the 16th/84th (~1SD) and 2.5th/97.5th (~2SD) percentiles of the predicted $\delta^{11}B_{CaCO3}$. (b) Logistic regression of $\delta^{11}B_{CaCO3}$ against weighted pH measurements. (c) Regression of $\delta^{11}B_{CaCO3}$ against the weighted DIC of jars.

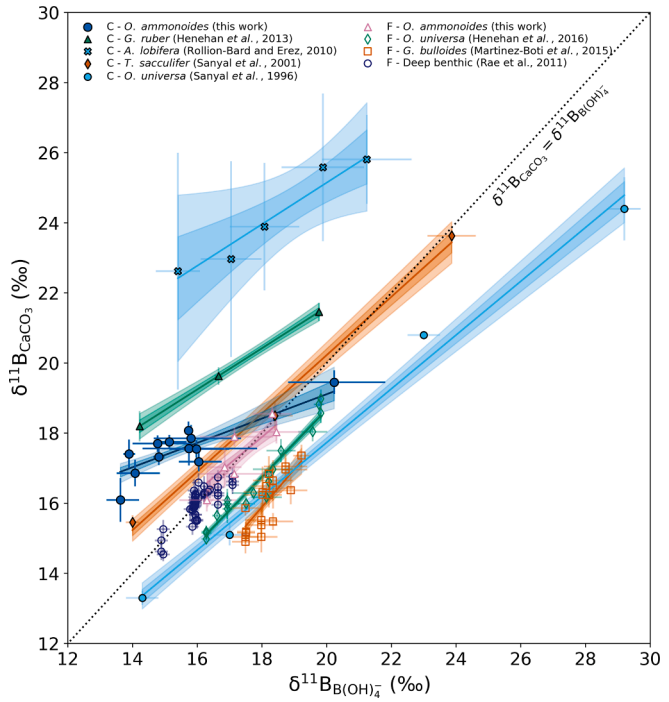

Fig. 3. Comparison of the *Operculina ammonoides* boron isotope calibration presented here to other foraminifera calibrations. *In situ* seawater $\delta^{11}B_{B(OH)4-}$ was calculated for the *Amphistegina lobifera* laboratory experiments using the information available in Rollion-Bard and Erez (2010), plotted against $\delta^{11}B_{CaCO3}$ based on the average and 2SE of all SIMS analysis available for a given experiment. The linear regression fit and statistics are all calculated using the Monte Carlo approach of this study (see text) such that the regression confidence intervals shown here may differ from those originally reported. The first letter of the legend refers to the calibration approach for each study, open symbol and F for the field samples while a closed symbol and the letter "C" represents calibrations based on laboratory cultured foraminifera.

$\delta^{11}B_{CaCO3}$, the DIC concentration in the growth media does not appear to have a significant influence on the $\delta^{11}B$ composition of cultured *O. ammonoides,* a simple OLS yields the following statistics: $R^2 = 0.04$, RMSE = 0.74 ‰, $p = 0.52$ (Fig. 2c).

The field collected specimens are characterised by measured $\delta^{11}B_{CaCO3}$ values ranging between 16.1 ‰ to 18.5 ‰ (Fig. 2, pink triangles) and their associated calculated *in situ* $\delta^{11}B_{B(OH)4-}$ range from 16.3 ‰ to 18.45 ‰. These samples have a notably different trend of boron isotopic composition compared to the cultured specimens as most seem to lie within uncertainty of the borate line. The linear regression performed using a Monte Carlo approach similar to that of the culture samples yields the following equation:

$$\delta^{11}B_{B(OH)_4^-} = \frac{\delta^{11}B_{CaCO_3} - \left(3.89^{+6.43}_{-8.50}\right)}{0.78^{+0.49}_{-0.37}} \quad (2)$$

Based on a simple least-square regression, the goodness of fit statistics are as follows: $R^2 = 0.74$, Root Mean Square Error (RMSE) is 0.43 ‰, and p=0.03. With a gradient within uncertainty of the borate line ($0.78^{+0.49}_{-0.37}$), the calcite $\delta^{11}B$ of field collected *O. ammonoides* appears to be more pH sensitive compared to the cultured specimens.

3.2. Comparison to other key proxy archives

With a gradient of $0.38^{+0.12}_{-0.10}$ the calibration of cultured *Operculina ammonoides* appears to have one of the shallowest slopes when compared to previously published calibrations (Fig. 3). Although most of the previously published culture calibrations are less pH sensitive than $B(OH)_4^-$: *Amphistegina lobifera* (0.59 ± 0.28, Rollion-Bard and Erez, 2010), *Orbulina universa* (0.77 ± 0.07, Sanyal et al., 1996), *Trilobatus sacculifer* (0.83 ± 0.07, Sanyal et al., 2001), *Globigerinoides ruber* (0.60 ± 0.08, Henehan et al., 2013), only the calibration of *A. lobifera* has a gradient within uncertainty to that of cultured *O. ammonoides*.

However, previous calibration of field collected specimens appear to be characterised by a $\delta^{11}B_{B(OH)4-} - \delta^{11}B_{CaCO3}$ gradient closer to 1: *Orbulina universa* (0.95 ± 0.17, Henehan et al., 2016), *Globigerina bulloides* (1.07 ± 0.25, Martínez-Botí et al., 2015) and the epifaunal deep benthic foraminifera *Cibicidoides wuellerstorfi, Cibicidoides mundulus* and *Planulina ariminensis* (Rae et al., 2011) which all lie on or in close vicinity to the boron isotopic composition of $B(OH)_4^-$. In the case of *O. ammonoides*, we also observe a steeper slope in field collected versus laboratory cultured specimens, with all samples falling within uncertainty of $\delta^{11}B_{B(OH)4-}$.

3.3. B/Ca

The B/Ca ratio is shown as a function of various aspects of calcite, seawater carbonate, and seawater boron chemistry to explore the possible influences on boron incorporation in *Operculina ammonoides* in Fig. 4. The measured B/Ca of cultured *O. ammonoides* ranges between 211 and 454 µmol/mol (lowest and highest pH experiment, respectively). These concentrations are significantly higher than most planktonic foraminifera species (40–110 µmol/mol for a range of planktonic species, see Henehan et al. (2016) and references therein) and deep benthic foraminifera (120 to 200 µmol/mol, Rae et al., 2011) but close to other symbiont-bearing benthic foraminifera (*Amphistegina lessonii* and *Aphistegina lobifera*, 70–590 µmol/mol; Levi et al. (2019)). We focus mainly on the possible relationship to $[B(OH)_4^-]$, since this is likely to be the dominant form of dissolved boron incorporated in the foraminifer's shell and therefore one of the main controls on the shell B/Ca (e.g. Hemming and Hanson, (1992); Klochko et al., (2009); Branson et al., (2015)). However, because $B(OH)_4^-$ competes with CO_3^{2-} or HCO_3^- for the anion position in the lattice, controls on B/Ca may be best described by some combination of $B(OH)_4^-$ and either DIC, HCO_3^- or CO_3^{2-} (Allen et al., 2011; Foster, 2008; Haynes et al., 2017; Yu et al., 2007; Yu and Elderfield, 2007). Therefore we also explore the degree to which combined aspects of the seawater carbonate and boron systems can explain variations in *O. ammonoides* B/Ca.

We observe very limited residual variance between the linear regression model and data for the measured B/Ca and $\delta^{11}B_{CaCO3}$ when including the field collected samples (Fig. 4a, R2 = 0.77, RSE= 0.38 ‰, $p = 2{\cdot}10^{-6}$), with two noticeable outliers, discussed in section 4.1. When only considering the cultured *O. ammonoides*, we find that this is reduced even further ($R^2 = 0.91$, RSE= 0.24 ‰, $p = 7{\cdot}10^{-6}$). The weighted jar pH and the calculated $[B(OH)_4^-]$ (Fig. 4b and c) can also explain a large portion of the variance in the B/Ca data, with B/Ca characterised by a tighter relationship with $[B(OH)_4^-]$ than pH. The B/Ca of *O. ammonoides* is also characterised by a significant linear relationship with $[B(OH)_4^-]$/[DIC] ($R^2 = 0.62$, RSE = 0.038 mmol/mol, $p = 0.004$). However, the B/Ca values from the constant pH, variable DIC experiment (Fig. 4d, orange squares) behave differently to the variable pH and $[Ca^{2+}]_{SW}$ experiments. The regression against $[B(OH)_4^-]$/[DIC] is very similar to that of $[B(OH)_4^-]/[HCO_3^-]$ since HCO_3^- represents between 84% (pH_{NBS} = 8.32) and 95% (pH_{NBS} = 7.49) of the total DIC. These results point towards a possible similarity on how *O. ammonoides* incorporates B compared to the planktonic foraminifera given that it has been shown that the amount of boron incorporated in the shell of planktonic species is best described by a $[B(OH)_4^-]$/carbonate chemistry ratio (Allen et al., 2011, 2016; Haynes et al., 2017). One notable difference is that no significant relationship between measured B/Ca and seawater DIC or $[Ca^{2+}_{SW}]$ is observed in the case of cultured *O. ammonoides* (Fig. S10), unlike planktonic foraminifera which have been shown in most cases to scale negatively with seawater DIC and (in some cases) positively with $[Ca^{2+}]$ (Haynes et al., 2017). Although the $[B(OH)_4^-]/[CO_3^{2-}]$ ratio has

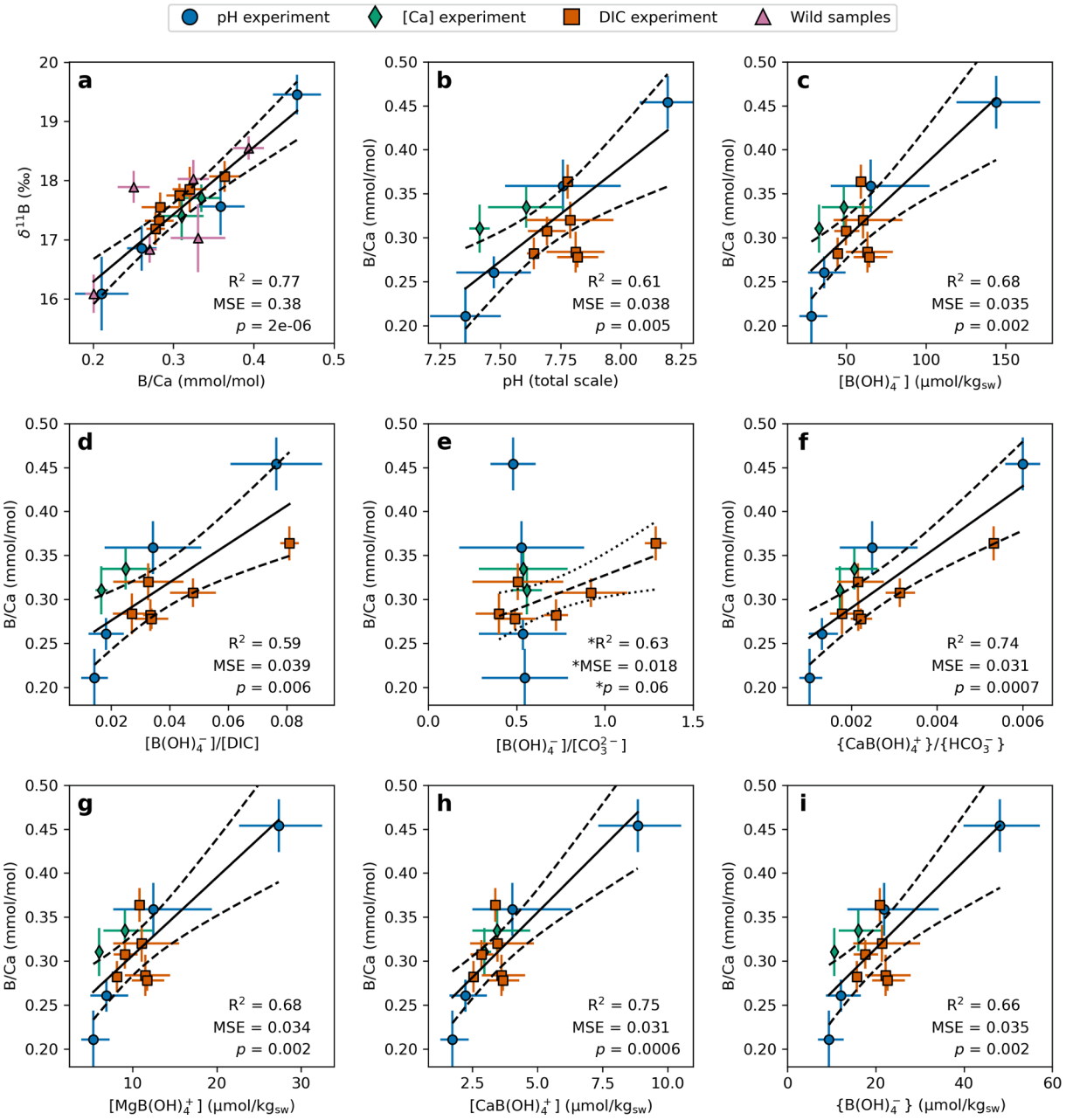

Fig. 4. The relationship between *Operculina ammonoides* B/Ca and different aspects of the seawater carbon/boron system. (a) The regression of $\delta^{11}B_{CaCO3}$ and measured B/Ca is characterised by a significant linear relationship, hinting towards a common underlying driving factor. The field collected specimens (pink triangles) were included in the regression. (b) Regression of B/Ca against the weighted pH of the culture jars. (c-e) Regression of B/Ca against different aspects of the seawater carbonate and boron system calculated using PyCO2SYS. The regression between B/Ca and $[B(OH)_4^-]/DIC$, which potentially accounts for competition between carbon and boron species for the anion position in the lattice, appears slightly less significant than that based on the concentration of $[B(OH)_4^-]$ alone. (f-i) B/Ca regressed against the concentration and activity of key boron species calculated using PHREEQC. The linear regression between B/Ca and calculated $[B(OH)_4^-]/[CO_3^{2-}]$(e) and statistics quoted in that panel only includes data from the DIC experiment (orange squares). The dotted lines represent the 95 % CI of the OLS fit. Linear regression statistics including the field collected samples are available in the supplementary materials (Fig. S9).

also been proposed as a controlling factor for B incorporation in planktonic foraminifera (Howes et al., 2017), its predictive power when considering planktonic foraminifera shell data seems mixed when pH and DIC are decoupled (Allen et al., 2012; Haynes et al., 2017). This variable ability of various carbonate system parameters to explain B incorporation in *O. ammonoides* also seems to be the case since the regression of B/Ca against $[B(OH)_4^-]/[CO_3^{2-}]$ is not significant ($R^2 = 0.023$, $p = 0.6$) when considering both the variable pH and variable DIC experiments. However, when considering the variable DIC experiment alone (HH7), with a wider range of $[CO_3^{2-}]$ (45 and 157 µmol/mol), a more significant positive trend becomes apparent (Fig. 4e, starred statistics; $R^2 = 0.63$, RSE = 0.018 mmol/mol, $p = 0.06$).

The results of the PHREEQC-derived ion pair calculations are shown in Fig. 4f-i. This analysis shows that there is a significant relationship between B/Ca and the $MgB(OH)_4^+$ (Fig. 4g) and $CaB(OH)_4^+$ (Fig. 4h) ion pairs ($R^2 = 0.67$, $p = 0.001$, and $R^2 = 0.74$, $p = 0.0004$ respectively). The calculated $CaB(OH)_4^+$ concentration can explain more of the variance in the data compared to total $B(OH)_4^-$ (Fig. 4c), mainly because the experiments in which $[Ca_{SW}^{2+}]$ was varied (HH6-5 and HH6-6, green diamonds in Fig. 4) have a higher $[CaB(OH)_4^+]$, bringing those two data points closer to the x-axis value of the other experiments with similar B/Ca. Similarly, when comparing $[B(OH)_4^-]/[DIC]$ to the activity ratio of

{$CaB(OH)_4^+$}/{HCO_3^-}, the trend remains nearly identical, but the fitting statistics are slightly improved since the {$CaB(OH)_4^+$} values of the higher [Ca^{2+}_{SW}] experiments bring those two point closer to others, whilst the rest of the dataset is uniformly transformed (Fig. 4f). The regression between B/Ca and the activity of $B(OH)_4^-$ (Fig. 4i) is very similar to that alternatively using the total concentration of $B(OH)_4^-$ (Fig. 4c), suggesting that minor differences in the boron activity coefficients between the experiments cannot explain a substantial portion of the variance in the data, although we note that regressions based on borate ion pairs/carbon system ratios or Ca^{2+}-borate ion pair alone do result in lower degrees of unexplained variance in the regressions.

4. Discussion

4.1. Boron incorporation in Operculina ammonoides

Our results show that, the incorporation of boron into *Operculina ammonoides* is dominantly driven by the carbonate system, with $\delta^{11}B$ principally dependent on pH and the overall B/Ca dataset most closely correlated to $B(OH)_4^-$ or a borate-containing ion pair (Fig. 4).

Specifically, *O. ammonoides* B/Ca is most tightly correlated with the calculated $CaB(OH)_4^+$ ion pair concentration of seawater ($R^2 = 0.75$, MSE = 31 μmol/mol, $p = 6{\cdot}10^{-4}$; Fig. 4h), though we note that $CaB(OH)_4^+$ only results in a slightly better fit to the B/Ca data compared to $MgB(OH)_4^+$ and total $B(OH)_4^-$ (Fig. 4g and c). Indeed, the slightly improved fit based on $CaB(OH)_4^+$ or $CaB(OH)_4^+/HCO_3^-$ may well not imply mechanistic involvement of the Ca ion pair, since all experiments except HH6-5 and HH6-6 had the same [Ca^{2+}_{SW}], and these two experiments were also conducted at slightly different average pH (green diamonds on Fig. 4). We note that Henehan et al. (2022) hypothesised that positively charged $CaB(OH)_4^+$ and $MgB(OH)_4^+$ ion pairs could migrate towards the growing crystal surface which has a negative electrostatic potential, repelling $B(OH)_4^-$ (Branson, 2018a), which warrants further study. However, as in the case of the $CaB(OH)_4^+$ ion pair, we cannot robustly assess the potential involvement of the $MgB(OH)_4^+$ in boron incorporation because [Mg^{2+}_{SW}] was similar in all experiments, such that the regression statistics when comparing B/Ca against [$MgB(OH)_4^+$] and [$B(OH)_4^-$] are nearly identical (Fig. 4g and c) as both parameters are driven by [$B(OH)_4^-$].

In addition, it has been hypothesized that the $NaB(OH)_4$ ion pair may play an important role in boron incorporation into calcite (Mavromatis et al., 2021). However, to our knowledge, no pitzer parameter exists for the $NaB(OH)_4$ ion pair, although a dissociation constant is available for the Minteq.v4 PHREEQC database (Pokrovski et al., 1995), which is intended for solutions with lower ionic strength (I<0.5; Allison et al. (1991)). Consequently, we did not explore the possibility of $NaB(OH)_4$ as a driver of boron incorporation for *O. ammonoides*. Irrespective, there were no substantial changes in [Na^+_{SW}] in our experiments, and unlike [Ca^{2+}_{SW}] and [Mg^{2+}_{SW}], [Na^+_{SW}] varied by no more than a few percent during the Cenozoic (Zeebe and Tyrrell, 2019), such that explaining foraminiferal B/Ca as a function of [$NaB(OH)_4$] rather than [$B(OH)_4$] makes little practical difference. Indeed, a $NaB(OH)_4$-B/Ca regression through our experimental data would almost certainly appear similar to [$B(OH)_4^-$] versus B/Ca (Fig. 4c), which means that we cannot identify the importance or otherwise of this ion pair on foraminiferal boron uptake.

Although we show that [$B(OH)_4^-$] or related ion pairs of the culture seawater appears to be the best predictor of the overall B/Ca dataset of the cultured *O. ammonoides*, it is worth noting that the constant pH variable DIC experiment (HH7, orange squares) shows a noticeably different trend when regressing their measured B/Ca against [$B(OH)_4^-$]/DIC (Fig. 4d), given that this metric has been extensively considered in previous studies. As such, although *O. ammonoides* appears to be characterised by a different sensitivity to DIC and [$B(OH)_4^-$]/DIC compared to planktonic foraminifera, in which this parameter has been considered as a major control on boron incorporation into shell calcite (Allen et al., 2012; Henehan et al., 2015; Haynes et al., 2017, 2019), [$B(OH)_4^-$]/DIC could nonetheless represent an important control on boron incorporation in *O. ammonoides*, albeit less so than [$B(OH)_4^-$] and related ion pairs.

The correlation between the measured $\delta^{11}B$ and measured B/Ca of a set of foraminifera can also provide information on the incorporation of B into the foraminifer's shell (Branson, 2018a). Indeed, if the isotopic composition scales with the concentration within the shell, it suggests that similar processes control both the shell boron concentration and isotopic fractionation. It has been suggested that $B(OH)_4^-$ is the main form of B being sampled and incorporated in the lattice (Hemming and Hanson, 1992; Klochko et al., 2009), although this remains to be studied in detail for most species (Branson et al., 2015). However, if both $\delta^{11}B$ and B/Ca increase as pH increases (Fig. 2b and 4b), and both strongly correlate with each other (Fig. 4a), it suggests, at the very least, that a substantial portion of the boron incorporated into the foraminifer's lattice is derived from $B(OH)_4^-$. Moreover, the fact that there is less unexplained variance in a regression between shell B/Ca and $\delta^{11}B$ compared to $\delta^{11}B_{CaCO3} - \delta^{11}B_{B(OH)4-}$ suggests that the additional unexplained variance in the latter case is derived from the measurement of seawater parameters (e.g. differential boundary layer versus bulk seawater carbonate chemistry, discussed in detail below).

The measured B/Ca of the field collected specimens fall within the range of the cultured *O. ammonoides* (ranging from 200 (SER) to 393 μmol/mol (SSO7G14)). However, when comparing their measured B/Ca with $\delta^{11}B$ measurements, not all samples fall within the observed close fit of the culture experiments, with two noticeable outliers (Fig. 4a). Given that the boron isotope and trace element measurements were not performed on the same specimens, but on the same sample population, it is possible that geochemical heterogeneity within the sample population is a source of bias in some cases, especially for samples from environments characterised by intra/interannual variability.

Overall, the B/Ca and $\delta^{11}B$ data strongly suggest that [$B(OH)_4^-$] or a closely related parameter controls boron incorporation into this species both in the field and in laboratory cultures (Fig. 4). Given that is the case, in the next section we explore why our laboratory culture calibration of the relationship between $\delta^{11}B_{CaCO3}$ and $\delta^{11}B_{B(OH)4-}$ is characterised by a much shallower slope and more positive $\delta^{11}B_{CaCO3}$ values than samples collected from the field.

4.2. Low pH sensitivity of cultured Operculina ammonoides

The laboratory culture gradient of the relationship between measured $\delta^{11}B_{CaCO3}$ and *in situ* $\delta^{11}B_{B(OH)4-}$ is substantially lower than 1 (Fig. 2a), unlike the field collected samples which appear to be characterised by a relationship with a gradient within uncertainty of 1 (Fig. 2a), indicating that that some process other than bulk seawater pH influences the boron isotopic composition of cultured *Operculina ammonoides* (Although the trend between measured $\delta^{11}B_{CaCO3}$ and $\delta^{11}B_{B(OH)4-}$ for the field collected samples is less well constrained compared to the culture sample set as discussed in section 2.3). This has been observed in other culture calibrations of both benthic and planktonic symbiont bearing foraminifera (Rollion-Bard and Erez, 2010; Henehan et al., 2013). One hypothesis to explain this discrepancy was proposed by Hönisch et al., (2019) in which a temperature dependent boron fractionation factor (α_B) would result in a shallower slope in the field collected calibration, thus matching the generally shallower slope of culture experiments. In order to explore this, we performed a correction using the equation in section 2.4.8 in Hönisch et al. (2019) and found a maximum difference in $\delta^{11}B_{B(OH)4-}$ of ~−0.31 ‰ for the highest temperature samples, see Fig. S14. However, the magnitude of this potential source of offset alone cannot explain the apparent trend difference between the field collected and cultured *O. ammonoides*.

It has been previously shown that symbiont bearing planktonic foraminifera do alter their micro-environment considerably via a combination of calcification, respiration and photosynthesis (Jørgensen et al., 1985; Rink et al., 1998; Erez, 2003; Köhler-Rink and Kühl, 2005; Glas et al., 2012b). On one hand calcification and respiration acidifies

the surrounding micro-environment of the calcifying organism, also known as the diffusive boundary layer (DBL) (Wolf-Gladrow et al., 1999; Zeebe and Wolf-Gladrow, 2001; Erez, 2003; Glas et al., 2012b, a; Toyofuku et al., 2017), whereas photosynthesis by the symbionts consumes CO_2, raising the microenvironment pH (Erez, 2003; Glas et al., 2012a). In general, there is a net increase in pH in the DBL during the day since photosynthesis prevails over the acidifying effects of calcification and respiration (Rink et al., 1998; Köhler-Rink and Kühl, 2000, 2005; Oron et al., 2020). During the night, calcification and respiration continues while photosynthesis does not take place, leaving a net decrease in the pH of the DBL relative to bulk seawater. Since the rate of photosynthesis in cultured *O. ammonoides* is not impacted by changing pH or DIC (Oron et al., 2020), the pH increase during the day is relatively constant at different surrounding pH and DIC concentrations. In contrast, calcification rates decrease at lower seawater pH (Oron et al., 2020), such that, taken together, it is expected that the net pH elevation in the DBL of cultured *O. ammonoides* increases as seawater pH decreases.

This effect may be exacerbated in our experiments because the size of the DBL of the cultured *O. ammonoides* may have been larger compared to field collected specimens since there was no water flow in the jars (Köhler-Rink and Kühl, 2000; Glas et al., 2012a; Toyofuku et al., 2017). This is supported by the experimental DBL measurements of Köhler-Rink and Kühl (2000), who showed that the size of the DBL of three LBF species (including a hyaline foraminifer) increased by a factor of four (from ~100 to ~400 μm) when there was no water flow, with an increase in DBL pH of ~0.2 between surrounding seawater and the foraminifer's surface when no flow was present. If *O. ammonoides* cultured in this way do indeed have a larger DBL than field collected samples, and if the seawater within the DBL is more alkaline at lower seawater pH as a result of a lower calcification rate under these conditions, then this might act as a strong dampening mechanism against changes in surrounding pH which could in turn explain the shallower gradient observed in the boron isotope calibration.

Oron et al. (2020) showed that *O. ammonoides* calcifies substantially more during the day than at night. Specifically, cultured *O. ammonoides* calcified 29 ± 7 % less on average in the dark. This means that around two thirds of the test of *O. ammonoides* should reflect calcification under light conditions, where photosynthesis results in a higher DBL pH, such that $\delta^{11}B_{B(OH)4-}$ in the boundary layer is more positive than that of the surrounding $\delta^{11}B_{B(OH)4-}$ especially at lower seawater pH values when calcification is inhibited relative to photosynthesis.

The reduced size of the DBL by water flow/turbulence could explain why the field collected specimens appear to be more sensitive to pH, as their microenvironment chemistry is controlled to a lesser extent by fluxes from the organism and more by the composition of the surrounding seawater. The lower DBL thickness would then mean that field collected *O. ammonoides* would sample seawater with physical and chemical properties much closer to that of their bulk environment. Although planktonic foraminifera have a different physiology, previous work seems to point towards this phenomenon. Indeed, most calibrations based on field collected specimens appear to be characterised by $\delta^{11}B_{B(OH)4-}$-$\delta^{11}B_{CaCO3}$ gradients of ~1, while most culture calibrations have a shallower slope (including of the same species, where data exists; Fig. 3). Rae (2018) suggested that in some instances, such as the culture calibration of *Orbulina universa* of Sanyal et al. (1996), part of the offset to lower $\delta^{11}B$ at higher pH in cultures may be explained by a simple assumption of calcification as a function Ω_c, which has a wide range in some culture experiments (e.g. ~1.5–20 in Sanyal et al. (1996)) compared to surface ocean waters (~4–7; e.g. Ridgwell, (2005)). This, in combination with the DBL diffusion effect described above, could drive the pH and $\delta^{11}B_{B(OH)4-}$ of the cultured micro-environment much lower than seawater at high pH, which would explain the greater deviation between the measured $\delta^{11}B_{CaCO3}$ and $\delta^{11}B_{B(OH)4-}$ of samples cultured at higher pH in the experiments of Sanyal et al. (1996). This shows that although some boron isotope pH calibrations of cultured foraminifera display a lower than expected pH sensitivity in the absence of any vital effects, they can record faithfully $\delta^{11}B_{B(OH)4-}$, but rather that of a more or less heavily altered micro-environment which may not be applicable to field collected specimens.

It is for these reasons that, in the next section, we model the DBL of *O. ammonoides* to explore in detail the possible factors which would result in the observed shallower calibration slope of cultured specimens compared to the near 1:1 relationship that characterises the field collected samples.

4.3. Micro-environment modelling

We postulated in the previous section that a likely driver for the observed shallow gradient between the measured $\delta^{11}B$ of cultured *O. ammonoides* and the calculated $\delta^{11}B_{B(OH)4-}$ of the seawater in which they grew is related to a larger than natural diffuse boundary layer (DBL) originating from the quiescent conditions of the laboratory culture. Although nummulitids (including *Operculina ammonoides*) are most abundant between depths of 10–40 m, which is typically characterised by a relatively low flow rate compared to the surface (< 0.1 m/s water flow) (Hansen and Buchardt, 1977; Hohenegger et al., 1999; Renema, 2002). The presence of a water flow, even if very low (< 1 cm/s), has been shown to significantly reduce the size of the DBL on some LBF (Köhler-Rink and Kühl, 2000). Conversely, a lack of flow would result in a larger DBL (Rink et al., 1998; Köhler-Rink and Kühl, 2000; Glas et al., 2012a). During our culture experiment, the seawater of the culture jars was quiescent in between water changes which we performed every 10 days, potentially resulting in conditions resulting in a larger than natural DBL. Since we did not use micro-sensors to measure the seawater chemistry at the surface of the shell of the cultured *O. ammonoides* but only measured bulk seawater chemistry from the culture jars, we instead opted to use a DBL model to explore the effects of a larger than natural DBL on the $\delta^{11}B_{B(OH)4-}$ at the surface of the shell on a population scale.

Modelling the micro-environment of calcifying organisms has previously shed light on laboratory culture pH – $\delta^{11}B$ calibrations to show that, in some cases, it is the boron isotopic composition of $B(OH)_4^-$ in the organism's micro-environment altered by life processes that is recorded (Zeebe et al., 2003; Rae, 2018). Thus, we aim to use a previously published DBL model to explore how specimens of *O. ammonoides* living in their natural habitat might have a physically and chemically distinct micro-environment compared to specimens cultured within a laboratory, and how this difference could explain the observed shallower gradient of the cultured *O. ammonoides*. We stress that we use this model to determine whether the offsets that we observe between $\delta^{11}B_{CaCO3}$ and *in situ* $\delta^{11}B_{B(OH)4-}$ are of the magnitude that we might expect given a pH-dependent change in calcification rate, rather than to constrain the necessary rates of these processes and/or DBL thickness required to explain the details of our dataset. The model employed here was developed by Wolf-Gladrow et al. (1999), and later updated by Zeebe et al. (2003) to include boron isotopes. This model requires the following inputs: foraminifer geometry, seawater physical and chemical parameters (temperature, salinity, pH, alkalinity or DIC) and carbon fluxes at the surface of the foraminifer, appropriate values of which were determined using the available data for this species and measurement of the laboratory culture parameters (see supplementary materials for a more detailed explanation of the derivation of those parameters).

For the purposes of the model, it was assumed that all fluxes took place directly at the surface of the shell, but we acknowledge this as a caveat because the chemistry alteration due to the presence of photosymbionts in *O. ammonoides* may remain internal; this potential issue is discussed in more detail below.

The diffusion–reaction model allows the different fluxes to be selectively added or removed to study their individual and combined impact on the seawater chemistry of the DBL (Fig. 5). Fig. 5a shows the reconstructed pH at the surface of the foraminifera both from the diffusion–reaction model and the measured boron isotopes (assuming

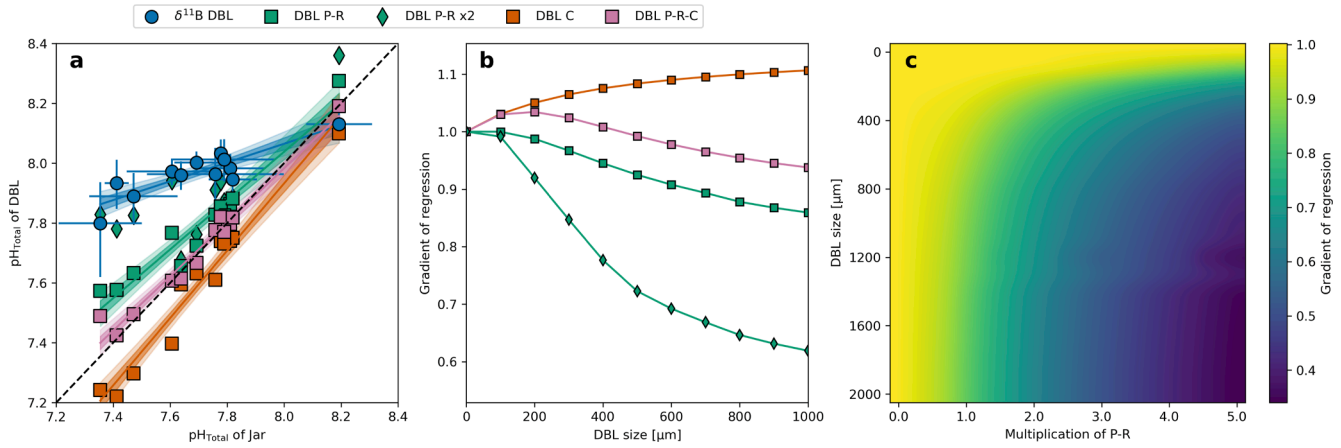

Fig. 5. Modelled and estimated pH of the microenvironment of *Operculina ammonoides*. (a) Estimated DBL pH as a function of weighted jar pH. pH reconstructed using $\delta^{11}B_{CaCO3}$ was made using the assumption of $\delta^{11}B_{CaCO3} = \delta^{11}B_{B(OH)4-}$ (see text). The calculation was performed using the Monte Carlo-simulated $\delta^{11}B_{B(OH)4-}$ converted to pH using the calculated pK_B^* and equation 5.10 from Rae (2018). The displayed points are the median of the Monte Carlo datasets and the uncertainties are the 2.5th and 97.5th percentiles. The different coloured squares represent the modelled pH of the DBL at the surface of the foraminifera, see legend (P = photosynthesis, R = respiration, C = calcification). In green, the fluxes at the surface were modelled considering only the balance between photosynthesis and respiration, in orange, only calcification and in pink, all three processes. The green diamonds represent model simulations in which the P-R carbon flux is doubled. All fluxes were estimated using the culture jars chemistry (see text). An OLS regression was calculated for each set of simulations, with 1 and 2SD confidence intervals of the fit displayed by the shaded regions. A DBL size of 1000 µm was used for the model. (b) Gradient of the OLS fit between modelled micro-environment pH and the bulk pH of the culturing medium as a function of DBL size (i.e. the sensitivity of the slope of the regression shown in panel a to the choice of DBL thickness). The fluxes were kept the same as in panel (a) and only the size of the DBL was changed. The colours of the lines follow the same colour code as panel (a). (c) Modelled gradients of the OLS fit between DBL pH and bulk pH as a function of DBL size and P-R flux. The P-R flux is displayed as a multiplicative factor, one being the calculated P-R rate based on jar chemistry measurements, two being twice the calculated flux, etc. For this plot, only the pH experiment HH6-1 to 4 were used for the model simulations.

$\delta^{11}B_{CaCO3} = \delta^{11}B_{B(OH)4-}$) as a function of mean culture jar pH experienced by the foraminifera (weighted average of pH). Foraminifera from all experiments but that conducted at the highest pH (HH6-4: $pH_T \approx 8.20$) are characterised by a boron isotopic composition indicative of a pH significantly higher than surrounding seawater. The estimated surface pH from the measured $\delta^{11}B$ of the shell of these experiments are closer to the photosynthesis driven modelled micro-environment. Inversely, the higher pH experiment (HH6-4: $pH_T \approx 8.20$) appears to record a micro-environment pH closer to a modelled DBL dominated by calcification. A similar observation was made by Rae (2018) when modelling the micro-environment $\delta^{11}B_{B(OH)4-}$ of the cultured *O. universa* of Sanyal et al. (1996) who suggested that the higher pH experiments were characterised by $\delta^{11}B_{CaCO3}$ close to modelled $\delta^{11}B_{B(OH)4-}$ when scaling calcification with $\Omega_{calcite}$. Nonetheless, we note that the reconstructed DBL pH of the lower pH experiments, using the calculated average fluxes, is not within the uncertainty of the modelled pH, possible reasons for which are discussed in detail below.

By varying the size of the DBL and keeping the carbon fluxes and the geometry constant, we can investigate how the pH of seawater at the surface of the foraminifera responds to an increasingly reaction-driven flux of carbon at the surface. As an example, Fig. 5b shows the variation of the gradient of linear regression between reconstructed DBL pH and pH of a culture medium (as illustrated in Fig. 5a) as a function of DBL size under different carbon flux scenarios. A difference in the gradient of the regression between a calcification only and P-R only scenario becomes noticeable beyond a DBL size of few hundred µm, after which the difference increases until it reaches a pseudo-plateau (Fig. 5b). To understand why this is, consider the case of the lowest pH experiment (HH6-1), which has a calculated average P-R rate of ~3.32 nmol C/h/individual, greater than the average calcification rate of ~0.81 nmol C/h/individual. In this case, the consumption of CO_2 outweighs its release in the DBL such that the pH at the surface of the foraminifer is higher than the surrounding seawater. When the DBL is larger, the surface of the cultured foraminifera would be more depleted in CO_2, but because diffusion happens more slowly than the flux of carbon at the surface, the main CO_2 source would be from the re-equilibration of CO_3^{2-} to HCO_3^-, which consumes a proton and increases pH. Inversely, when the DBL is smaller, CO_2 readily diffuses to replenish the surface layer, and thus the surface pH increase is less pronounced. In the case of the highest pH experiment (HH6-4), the estimated photosynthesis minus respiration rate of ~3.32 nmol C/h/individual is close to the calculated average rate of calcification (~3.57 nmol C/h/individual). As such, unlike the low-pH experiment HH6-1, there is a net release of CO_2 in the DBL and the seawater at the surface of the foraminifera will be more acidic. This explains why, when combining all the fluxes (pink squares), the resulting surface pH of the DBL is close to the surrounding seawater pH, since the fluxes broadly cancel out. Beyond a certain DBL size, the changes in micro-environment pH plateau as the DBL becomes increasingly reaction driven rather than diffusion dominated, ultimately becoming insensitive to DBL thickness at width >1000 µm.

If the P-R is doubled (Fig. 5a, green diamonds), the simulated pH of the DBL, using the previously mentioned assumptions and parameters, lies within the uncertainty of the calculated DBL pH using the $\delta^{11}B$ measurements. Although it is worth noting that this is only the case for the variable pH experiments (HH6) as we consider our estimates of P-R to be unrealistic in the case of the variable DIC experiments (HH7), see Figure S12. Because the calculated P-R rates are only an average of over 30 days, the actual fluxes during the day might be higher, hinting towards a photosynthesis driven DBL for our experiments.

We again stress that we use the model to investigate the likely direction of pH modification in the DBL rather than the precise details of our experiments, such that the details of the results of the diffusion–reaction model of the micro-environment presented here should be viewed within the context of a number of caveats and simplifying assumptions:

- The model describes the chemistry of seawater in the DBL for fluxes averaged over a period of weeks, such that it is important to note that the model cannot capture the variability of these fluxes through time. For example, calcification is likely not a continuous process like respiration but a discrete event lasting a few hours every few days

(Erez, 2003; Glas et al., 2012b), the timing of which is difficult to constrain on a population level. This could mean that during a calcification event, the decrease in DBL pH would be stronger and thus record a boron isotopic composition lower than predicted, although a comparison of the calculated DBL pH from $\delta^{11}B_{CaCO3}$ to the model does not support this (Fig. 5). In addition, we note that genus *Operculina* is likely similar to other hyaline tropical benthic species in that it probably possesses an internal carbon pool and vacuolises seawater (ter Kuile and Erez, 1987; Erez, 2003; Bentov et al., 2009; de Nooijer et al., 2009; Evans et al., 2018a). This means that the process of chamber formation could be decoupled from the time at which seawater is vacuolised from around the organism. While there is evidence for light enhanced calcification (Erez, 2003; Oron et al., 2020) and respiration (Erez, 2003), hinting towards enhanced metabolic activity during the day, we cannot quantify their respective effects on the incorporation of boron in *O. ammonoides*.

- Hyaline foraminifera posses a dense pseudopodia network in proximity to their shell surface that is involved in feeding, respiration, movement, chamber formation, and excretion (Erez, 2003). In performing these functions, pseudopodia likely also alter the microenvironment of the LBF, which we cannot quantify.
- The pseudopodia are also responsible for the process of seawater vacuolisation by the foraminifera, such that this species may sample seawater that is not adjacent to the shell surface (Erez, 2003; Bentov et al., 2009).
- The pH of the vacuolised seawater is likely modified (increased) before it reaches the site of calcification (de Nooijer et al., 2008, 2009; Bentov et al., 2009). However, the boron isotopic composition recorded by *O. ammonoides* (and other foraminifera) broadly falls within a few permil of $\delta^{11}B_{B(OH)4-}$ at their respective seawater pH (see Fig. 4) and not at around 25 or 30 ‰ which would be the $\delta^{11}B_{B(OH)4-}$ of the alkalinised vacuoles or calcifying fluid (pH ≈ 9). It has been hypothesised that membrane-permeable boric acid facilitates isotopic equilibrium between the calcifying fluid with the surrounding seawater (Gagnon et al., 2021). If this is indeed the case the shell would still record the DBL $\delta^{11}B_{B(OH)4-}$.
- Our calculations assume only $B(OH)_4^-$ incorporation into calcite, which is not always the case in inorganic precipitation experiments (e.g. Noireaux et al., 2015; Henehan et al., 2022). Given that boric acid entrapment may be precipitation rate dependent (Branson, 2018a), this may additionally explain the higher reconstructed DBL pH in our lowest seawater pH experiments.

While these complicating factors warrant further study, *O. ammonoides* lives near the shallow reef base (Hohenegger et al., 1999; Renema, 2002), which is comparatively higher-energy environments when compared to the quiescence of laboratory cultures, such that possible differences in DBL thickness between specimens grown in culture and natural samples should be considered when utilising empirical calibrations. Previous experiments which introduced a unidirectional flow to the culture bath measured a DBL thickness of around 100 μm in hyaline LBF (Köhler-Rink and Kühl, 2000; Glas et al., 2012a). At this size, the diffusion reaction model predicts very modest changes compared to the bulk seawater, ranging from 0.03 units (HH6-4) to 0.05 units (HH6-1) in any of the calcification/photosynthesis/respiration scenarios. Applying this modelled non-significant DBL modification to field collected specimens could explain their $\delta^{11}B_{CaCO3}$ falling closer to calculated *in situ* $\delta^{11}B_{B(OH)4-}$, and also explains the offset that we observe between the calibration slope of field and laboratory cultured specimens.

In summary, the DBL diffusion–reaction model results demonstrate that carbonate chemistry in the boundary layer is strongly sensitive to the DBL thickness for fluxes relevant to *O. ammonoides*. Specifically, a thicker DBL in our laboratory culture experiments coupled with a photosynthesis-dominated DBL chemistry highlights the potential for important differences between field-collected and laboratory cultured $\delta^{11}B_{CaCO3}$ values at a given pH (Fig. 2), and potentially explains the shallow $\delta^{11}B_{CaCO3}$-$\delta^{11}B_{B(OH)4-}$ slope observed in our cultured specimens but not in field collected samples.

4.4. Implications for palaeo-pH reconstructions

The previous section explored, through modelling, how a larger than natural DBL could create an altered seawater layer around the cultured LBF. This layer would then be sampled for calcification during the culture experiments, such that the measured seawater parameters of the laboratory culture settings might not reflect the seawater used to create the shells of the LBF. This problem has also been observed for the well established and widely used planktonic foraminifera boron isotope calibrations (Hönisch et al., 2003; Henehan et al., 2013, 2016). Although the issue of the DBL chemistry resulting in a shell $\delta^{11}B$ offset compared to $\delta^{11}B_{B(OH)4-}$ has previously only been suggested in the case of the free floating planktic foraminifera (e.g. Zeebe et al., 2003; Henehan et al., 2016), we show here that symbiont bearing benthic foraminifera record $\delta^{11}B$ within uncertainty of $\delta^{11}B_{B(OH)4-}$ (as also previously shown in deeper benthic foraminifera, Rae et al., (2011)) except in the case of laboratory our cultured specimens, which are influenced by larger than natural DBL with carbonate chemistry modified by the life processes of the foraminifera. We stress that this is uniquely a problem for carbonate system-sensitive proxies and does not, as far as we are aware, have any implication for the large amount of laboratory culturing work that has focused on the calibration of (e.g.) the majority of trace element ratios.

Another important consideration when working with an empirical $\delta^{11}B$-pH calibration is its applicability to fossil samples through geological times. Most published foraminifera $\delta^{11}B$-pH empirical calibrations (both field collected and cultured) used species that have evolved since the late Oligocene, for instance: *Trilobatus sacculifer* (Sanyal et al., 2001; Foster, 2008; Martínez-Botí et al., 2015), *Globigerinoides ruber* (Foster, 2008; Henehan et al., 2013), *Neogloboquadrina pachyderma* (Yu et al., 2013; Henehan et al., 2016), *Globigerina bulloides* (Martínez-Botí et al., 2015), and *Orbulina universa* (Henehan et al., 2016) all originated in the late Oligocene to mid-Miocene (Kennett and Srinivasan, 1983; Spezzaferri et al., 2018). To use calibrations that by implication include foraminifera vital effects beyond the time of origination of the calibrated species necessitates careful consideration of indirect evidence of vital effects in extinct species, and is usually done by comparing the $\delta^{11}B$, $\delta^{13}C$, $\delta^{18}O$, and B/Ca of fossil foraminifera assemblages (Edgar et al., 2015; Anagnostou et al., 2016, 2020; Henehan et al., 2020). Because *Operculina ammonoides* originated in the late Palaeocene (Hottinger, 1977), our $\delta^{11}B$-pH calibration can be directly applied to well preserved fossil samples throughout most of the Cenozoic, without the need for complex assemblage analysis which induces uncertainty in the interpretation of the reconstructions.

The pH (total scale) range of our culture calibration extends from ~ 8.19 to ~ 7.35 (lowest pH experiment, HH6-1), which is similar to the pH of seawater reconstructed during peak high CO_2 hothouse climate episodes during the Cenozoic (Gutjahr et al., 2017; Harper et al., 2020; Henehan et al., 2020; Anagnostou et al., 2020; Rae et al., 2021). Using this extreme as an example, we briefly explore the hypothetical impact of applying our laboratory versus field calibration on samples of this age.

At its peak, the PETM was characterised by a seawater pH of ~7.4 (Gutjahr et al., 2017; Rae et al., 2021). Assuming this would result in a $\delta^{11}B_{B(OH)4-}$ ≈ 13 ‰ (with typical seawater conditions of the mid-latitude Eocene ocean; temperature ≈ 28 °C, salinity = 35 psu, $[Ca_{SW}]$ ≈ 17 mmol/kg, $[Mg]_{sw}$ ≈ 35 mmol/kg, $\delta^{11}B_{SW}$ ≈ 38.5 ‰ (Evans et al., 2018b; Zeebe and Tyrrell, 2019; Rae et al., 2021; CenCO2PIP et al., 2023) following Hain et al. (2015) and Zeebe and Tyrrell (2019) for chemical constant modifications with seawater chemistry), using our *O. ammonoides* laboratory culture calibration (Eq. (1)) to correct for vital effects would result in a reconstructed $\delta^{11}B_{B(OH)4-}$ of ~16.65 ‰. Using this value and the conditions listed above, we would reconstruct a

seawater pH (total scale) of ~7.98, which using a conservative estimate of alkalinity of 2330 μmol/kg (Rae et al., 2021), would yield pCO_2 of ~554 ppmv, compared to the estimated >2000 ppmv during peak warmth of the early Eocene (in the case of $\delta^{11}B_{CaCO3} = \delta^{11}B_{B(OH)4-}$). While this example is likely a worst-case thought experiment, as many calibrations are derived from field samples in which DBL thickness is not likely to change through time, it nonetheless serves to highlight the potential pitfalls of applying a laboratory boron system calibration to deep-time fossil samples or a modern field calibration to extinct species potentially characterised by differing vital effects. Given their long fossil record and $\delta^{11}B_{CaCO3}$ within uncertainty of $\delta^{11}B_{B(OH)4-}$ in natural settings, this immediately suggests that boron isotope measurements of well-preserved fossil *O. ammonoides* from this interval would be a fruitful line of enquiry in confirming whether current approaches applied to extinct planktonic foraminifera are robust.

Another factor that must be considered when deriving palaeo-pH/CO_2 reconstructions is the surface water CO_2 equilibrium with the overlaying atmosphere (Foster and Sexton, 2014; Martínez-Botí et al., 2015; Foster and Rae, 2016). As is also the case for regions of the open ocean (Takahashi et al., 2009), the surface ocean pCO_2 of shallow marine environments is often in disequilibrium, with some shallow reefs shown to be net emitters of CO_2 (positive ΔpCO_2; (Bates et al., 2001; Yan et al., 2018; Terlouw et al., 2019; Ko et al., 2024) and others the opposite (Shaw and McNeil, 2014; Ko et al., 2024). As in any study interpreting boron isotope data from fossil samples, this should be carefully considered before converting reconstructed $\delta^{11}B_{B(OH)4-}$ into pCO_2.

5. Conclusions

Here, we show how the use of LA-MC-ICPMS to selectively sample calcite precipitated during controlled laboratory culture experiments allows the relationship between the boron isotopic composition of the shell and pH to be calibrated in a species of larger benthic foraminifera. The results of this exercise demonstrate that cultured *Operculina ammonoides* is characterised by a $\delta^{11}B_{CaCO3}$-$\delta^{11}B_{B(OH)4-}$ slope substantially lower than 1. In contrast, natural specimens have a measured boron isotopic composition within uncertainty of calculated *in situ* $B(OH)_4^-$. We explored this discrepancy using a previously published diffusion–reaction model (Wolf-Gladrow et al., 1999), the results of which show that cultured *O. ammonoides* may be characterised by a shallow $\delta^{11}B_{CaCO3}$-$\delta^{11}B_{B(OH)4-}$ slope as a result of a strongly altered micro-environment because of a thick diffuse boundary layer in the quiescent laboratory culture conditions compared to specimens growing in the wild. Future culture studies should therefore be mindful of potential differences in the micro-environment of foraminifera between the laboratory and field, especially when interpreting geochemical data in light of carbonate/boron seawater chemistry, although we stress that this is likely to be a unique problem for carbonate chemistry sensitive proxies (in contrast to e.g. alkali/alkaline earth metals). Our field calibration paves the way forward for the use of this group of foraminifera for palaeo-pH/CO_2 reconstruction. In addition, B/Ca data show that boron incorporation in *O. ammonoides* is dominantly controlled by some aspect of seawater borate chemistry (e.g. $[B(OH)_4^-]$ or a borate ion pair). This potentially opens up the possibility of constraining multiple aspects of seawater carbonate chemistry by coupling this information to boron isotope measurements. More broadly, our results demonstrate that the nummulitid tropical shallow-dwelling foraminifera are a useful group of calcifiers for palaeoreconstruction using the data presented here, especially given that some genera, such as *Operculina,* are present throughout the majority of the Cenozoic.

Data availability

Data are available through Zenodo at https://zenodo.org/record/8246890.

CRediT authorship contribution statement

Douglas Coenen: Writing – original draft, Visualization, Software, Methodology, Investigation, Formal analysis, Data curation, Conceptualization. **David Evans:** Writing – review & editing, Validation, Supervision, Resources, Project administration, Methodology, Investigation, Funding acquisition, Conceptualization. **Hagar Hauzer:** Writing – review & editing, Resources, Methodology, Investigation. **Romi Nambiar:** Writing – review & editing, Resources, Methodology. **Hana Jurikova:** Writing – review & editing, Resources, Data curation. **Matthew Dumont:** Writing – review & editing, Resources, Data curation. **Puspita Kanna:** Writing – review & editing, Resources. **James Rae:** Writing – review & editing, Resources, Funding acquisition. **Jonathan Erez:** Writing – review & editing, Investigation, Funding acquisition. **Laura Cotton:** Writing – review & editing. **Willem Renema:** Writing – review & editing, Resources. **Wolfgang Müller:** Writing – review & editing, Supervision, Project administration, Investigation, Funding acquisition, Conceptualization.

Declaration of competing interest

The authors declare that they have no known competing financial interests or personal relationships that could have appeared to influence the work reported in this paper.

Acknowledgements

We thank Richard Zeebe and Dieter Wolf-Gladrow for providing their code for the diffusion-reaction model and Oscar Branson for providing the Python frontend. We thank Max Fursman for putting Puspita Kanna in touch with us for this collaboration. The foraminifera culturing was funded by NSF-BSF project 1634573 and by ISF project 790/16 and 1886/20 to Jonathan Erez. FIERCE is financially supported by the Wilhelm and Else Heraeus Foundation and by the Deutsche Forschungsgemeinschaft (DFG: INST 161/921-1 FUGG, INST 161/923-1 FUGG and INST 161/1073-1 FUGG), which is gratefully acknowledged. This research was funded through the VeWA research consortium (Past Warm Periods as Natural Analogues of our high-CO_2 Climate Future) by the LOEWE programme of the Hessen Ministry of Higher Education, Research and the Arts, Germany, and also by the RSE, Saltire International Collaboration Award number 1964. We would like to thank the editor, editor in chief, and two anonymous reviewers for taking the time and effort necessary to review the manuscript. We sincerely appreciate all valuable comments and suggestions, which resulted in a substantially improved version. This is FIERCE contribution No. 168.

Appendix A. Supplementary material

Supplementary figures and tables can be found in the supplementary materials accompanying this article. More information can be found on the analytical setup used for this study and the analysis done within the FIERCE laboratory. There is also further information on: i) the *O. ammonoides* culturing performed in the Institute of Earth Sciences at the Hebrew University of Jerusalem, ii) the culture seawater chemistry measurements, iii) the calcification and photosynthesis rate calculations, iv) alternative calculation scenarios for the calculated $\delta^{11}B_{B(OH)4-}$ of the cultured and field collected *O. ammonoides*, and v) the field collected samples as well as maps detailing the sampling location and seawater pH measurement locations. Files for the PHREEQC and diffusion-reaction model results can also be found. Supplementary material to this article can be found online at https://doi.org/10.1016/j.gca.2024.06.020.

References

Afdal, B.D.G., Wahyudi, A.J., Rastina, P.H.B., Hamzah, F., Koropitan, A.F., 2024. Spatial variability of aragonite saturation state (Ωarag) in Indonesian coastal waters. Mar. Environ. Res. 195, 106377.

Allen, K.A., Hönisch, B., Eggins, S.M., Yu, J., Spero, H.J., Elderfield, H., 2011. Controls on boron incorporation in cultured tests of the planktic foraminifer *Orbulina universa*. Geophys. Res. Lett. 309, 291–301.

Allen, K.A., Hönisch, B., Eggins, S.M., Rosenthal, Y., 2012. Environmental controls on B/Ca in calcite tests of the tropical planktic foraminifer species *Globigerinoides ruber* and *Globigerinoides sacculifer*. Earth Planet. Sci. Lett. 351–352, 270–280.

Allen, K.A., Hönisch, B., Eggins, S.M., Haynes, L.L., Rosenthal, Y., Yu, J., 2016. Trace element proxies for surface ocean conditions: a synthesis of culture calibrations with planktic foraminifera. Geochim. Cosmochim. Acta 193, 197–221.

Allison, J.D., Brown, D.S., Novo-Gradac, K.J., 1991. MINTEQA2/PRODEFA2, a Geochemical Assessment Model for Environmental Systems: Version 3.0 User's Manual. Environmental Research Laboratory, Office of Research and Development, U.S. Environmental Protection Agency.

Anagnostou, E., Huang, K.-F., You, C.-F., Sikes, E.L., Sherrell, R.M., 2012. Evaluation of boron isotope ratio as a pH proxy in the deep sea coral *Desmophyllum dianthus*: evidence of physiological pH adjustment. Earth Planet. Sci. Lett. 349–350, 251–260.

Anagnostou, E., John, E.H., Edgar, K.M., Foster, G.L., Ridgwell, A., Inglis, G.N., Pancost, R.D., Lunt, D.J., Pearson, P.N., 2016. Changing atmospheric CO_2 concentration was the primary driver of early Cenozoic climate. Nature 533, 380–384.

Anagnostou, E., John, E.H., Babila, T.L., Sexton, P.F., Ridgwell, A., Lunt, D.J., Pearson, P. N., Chalk, T.B., Pancost, R.D., Foster, G.L., 2020. Proxy evidence for state-dependence of climate sensitivity in the Eocene greenhouse. Nat. Commun. 11, 4436.

Barker, S., Greaves, M., Elderfield, H., 2003. A study of cleaning procedures used for foraminiferal Mg/Ca paleothermometry. Geochem. Geophys. Geosystems 4, 8407.

Bates, N.R., Samuels, L., Merlivat, L., 2001. Biogeochemical and physical factors influencing seawater fCO_2 and air-sea CO_2 exchange on the Bermuda coral reef. Limnol. Oceanogr. 46, 833–846.

Bentov, S., Brownlee, C., Erez, J., 2009. The role of seawater endocytosis in the biomineralization process in calcareous foraminifera. Proc. Natl. Acad. Sci. 106, 21500–21504.

Branson, O., 2018a. Chapter 4: Boron incorporation into marine $CaCO_3$. In: Marshall, H., Foster, G. (Eds.), Boron Isotopes. Springer, pp. 71–105.

Branson, O., Kaczmarek, K., Redfern, S.A.T., Misra, S., Langer, G., Tyliszczak, T., Bijma, J., Elderfield, H., 2015. The coordination and distribution of B in foraminiferal calcite. Earth Planet. Sci. Lett. 416, 67–72.

Branson, O., 2018b. oscarbranson/cbsyst: 0.4.5. https://doi.org/10.5281/zenodo.7620872. Accessed: 2023-02-08.

CenCO2PIP, Hönisch, B., Royer, D.L., Breecker, D.O., Polissar, P.J., Bowen, G.J., Henehan, M.J., Cui, Y., Steinthorsdottir, M., McElwain, J.C., Kohn, M.J., Pearson, A., Phelps, S.R., Uno, K.T., Ridgwell, A., Anagnostou, E., Austermann, J., Badger, M.P.S., Barclay, R.S., Bijl, P.K., Chalk, T.B., Scotese, C.R., De La Vega, E., DeConto, R.M., Dyez, K.A., Ferrini, V., Franks, P.J., Giulivi, C.F., Gutjahr, M., Harper, D.T., Haynes, L.L., Huber, M., Snell, K.E., Keisling, B.A., Konrad, W., Lowenstein, T.K., Malinverno, A., Guillermic, M., Mejía, L.M., Milligan, J.N., Morton, J.J., Nordt, L., Whiteford, R., Roth-Nebelsick, A., Rugenstein, J.K.C., Schaller, M.F., Sheldon, N.D., Sosdian, S., Wilkes, E.B., Witkowski, C.R., Zhang, Y.G., Anderson, L., Beerling, D.J., Bolton, C., Cerling, T.E., Cotton, J.M., Da, J., Ekart, D.D., Foster, G.L., Greenwood, D. R., Hyland, E.G., Jagniecki, E.A., Jasper, J.P., Kowalczyk, J.B., Kunzmann, L., Kürschner, W.M., Lawrence, C.E., Lear, C.H., Martínez-Botí, M.A., Maxbauer, D.P., Montagna, P., Naafs, B.D.A., Rae, J.W.B., Raitzsch, M., Retallack, G.J., Ring, S.J., Seki, O., Sepúlveda, J., Sinha, A., Tesfamichael, T.F., Tripati, A., Van Der Burgh, J., Yu, J., Zachos, J.C., Zhang, L., 2023. Toward a Cenozoic history of atmospheric CO_2. Science 382, eadi5177.

Cotton, L.J., Evans, D., Beavington-Penney, S.J., 2020. The high-magnesium calcite origin of Nummulitd foraminifera and implications for the identification of calcite diagenesis. PALAIOS 35, 421–431.

D'Agostino, R., Pearson, E.S., 1973. Tests for departure from normality. Empirical results for the distributions of b2 and sqrt b1. Biometrika 60, 613–622.

de Nooijer, L.J., Toyofuku, T., Oguri, K., Nomaki, H., Kitazato, H., 2008. Intracellular pH distribution in foraminifera determined by the fluorescent probe HPTS. Limnol. Oceanogr. Methods 6, 610–618.

de Nooijer, L.J., Toyofuku, T., Kitazato, H., 2009. Foraminifera promote calcification by elevating their intracellular pH. Proc. Natl. Acad. Sci. 106, 15374–15378.

Dickson, A.G., 1990. Thermodynamics of the dissociation of boric acid in synthetic seawater from 273.15 to 318.15 K. Deep Sea Res. Part Oceanogr. Res. Pap. 37, 755–766.

Dickson, A.G., Sabine, C.L., Christian, J.R., Bargeron, C.P., n.d. North Pacific Marine Science Organization (Eds.), 2007. Guide to best practices for ocean CO_2 measurements, North Pacific Marine Science Organization, Sidney, BC.

Edgar, K.M., Anagnostou, E., Pearson, P.N., Foster, G.L., 2015. Assessing the impact of diagenesis on $\delta^{11}B$, $\delta^{13}C$, $\delta^{18}O$, Sr/Ca and B/Ca values in fossil planktic foraminiferal calcite. Geochim. Cosmochim. Acta 166, 189–209.

Edwards, K.J., Valley, J.W., 1998. Oxygen isotope diffusion and zoning in diopside: the importance of water fugacity during cooling. Geochim. Cosmochim. Acta 62, 2265–2277.

Erez, J., 2003. The Source of Ions for Biomineralization in Foraminifera and Their Implications for Paleoceanographic Proxies. Rev. Mineral. Geochem. 54, 115–149.

Evans, D., Müller, W., Oron, S., Renema, W., 2013. Eocene seasonality and seawater alkaline earth reconstruction using shallow-dwelling large benthic foraminifera. Earth Planet. Sci. Lett. 381, 104–115.

Evans, D., Müller, W., 2018. Automated Extraction of a Five-Year LA-ICP-MS Trace Element Data Set of Ten Common Glass and Carbonate Reference Materials: Long-Term Data Quality, Optimisation and Laser Cell Homogeneity. Geostand. Geoanalytical Res. 42, 159–188.

Evans, D., Erez, J., Oron, S., Müller, W., 2015. Mg/Ca-temperature and seawater-test chemistry relationships in the shallow-dwelling large benthic foraminifera *Operculina ammonoides*. Geochim. Cosmochim. Acta 148, 325–342.

Evans, D., Brierley, C., Raymo, M.E., Erez, J., Müller, W., 2016. Planktic foraminifera shell chemistry response to seawater chemistry: Pliocene-Pleistocene seawater Mg/Ca, temperature and sea level change. Earth Planet. Sci. Lett. 438, 139–148.

Evans, D., Müller, W., Erez, J., 2018a. Assessing foraminifera biomineralisation models through trace element data of cultures under variable seawater chemistry. Geochim. Cosmochim. Acta 236, 198–217.

Evans, D., Sagoo, N., Renema, W., Cotton, L.J., Müller, W., Todd, J.A., Saraswati, P.K., Stassen, P., Ziegler, M., Pearson, P.N., Valdes, P.J., Affek, H.P., 2018b. Eocene greenhouse climate revealed by coupled clumped isotope-Mg/Ca thermometry. Proc. Natl. Acad. Sci. 115, 1174–1179.

Evans, D., Gerdes, A., Coenen, D., Marschall, H.R., Müller, W., 2021. Accurate correction for the matrix interference on laser ablation MC-ICPMS boron isotope measurements in $CaCO_3$ and silicate matrices. J. Anal. at. Spectrom. 36, 1607–1617.

Farmer, J.R., Branson, O., Uchikawa, J., Penman, D.E., Hönisch, B., Zeebe, R.E., 2019. Boric acid and borate incorporation in inorganic calcite inferred from B/Ca, boron isotopes and surface kinetic modeling. Geochim. Cosmochim. Acta 244, 229–247.

Foster, G.L., 2008. Seawater pH, pCO_2 and $[CO_3^{2-}]$ variations in the Caribbean Sea over the last 130 kyr: a boron isotope and B/Ca study of planktic foraminifera. Earth Planet. Sci. Lett. 271, 254–266.

Foster, G.L., Pogge von Strandmann, P.A., Rae, J.W.B., 2010. Boron and magnesium isotopic composition of seawater. Geochem. Geophys. Geosystems 11, Q08015.

Foster, G.L., Lear, C.H., Rae, J.W.B., 2012. The evolution of pCO_2, ice volume and climate during the middle Miocene. Earth Planet. Sci. Lett. 341–344, 243–254.

Foster, G.L., Rae, J.W.B., 2016. Reconstructing Ocean pH with Boron Isotopes in Foraminifera. Annu. Rev. Earth Planet. Sci. 44, 207–237.

Foster, G.L., Sexton, P.F., 2014. Enhanced carbon dioxide outgassing from the eastern equatorial Atlantic during the last glacial. Geology 42, 1003–1006.

Gagnon, A.C., Gothmann, A.M., Branson, O., Rae, J.W.B., Stewart, J.A., 2021. Controls on boron isotopes in a cold-water coral and the cost of resilience to ocean acidification. Earth Planet. Sci. Lett. 554, 116662.

Gatz, D.F., Smith, L., 1995. The standard error of a weighted mean concentration—I. Bootstrapping Vs Other Methods. Atmos. Environ. 29, 1185–1193.

Glas, M.S., Fabricius, K.E., Beer, D. de, Uthicke, S., 2012a. The O_2, pH and Ca^{2+} microenvironment of benthic foraminifera in a high CO_2 world. PLOS ONE 7, e50010.

Glas, M.S., Langer, G., Keul, N., 2012b. Calcification acidifies the microenvironment of a benthic foraminifer (*Ammonia sp.*). J. Exp. Mar. Biol. Ecol. 424–425, 53–58.

Graham, C.M., Valley, J.W., Eiler, J.M., Wada, H., 1998. Timescales and mechanisms of fluid infiltration in a marble: an ion microprobe study. Contrib. Miner. Pet. 132, 371–389.

Gregor, L., Gruber, N., 2021. OceanSODA-ETHZ: a global gridded data set of the surface ocean carbonate system for seasonal to decadal studies of ocean acidification. Earth Syst. Sci. Data 13, 777–808.

Griffiths, N., Müller, W., Johnson, K.G., Aguilera, O.A., 2013. Evaluation of the effect of diagenetic cements on element/Ca ratios in aragonitic Early Miocene (~16 Ma) Caribbean corals: implications for 'deep-time' palaeo-environmental reconstructions. Palaeogeogr. Palaeoclimatol. Palaeoecol. 369, 185–200.

Gutjahr, M., Ridgwell, A., Sexton, P.F., Anagnostou, E., Pearson, P.N., Pälike, H., Norris, R.D., Thomas, E., Foster, G.L., 2017. Very large release of mostly volcanic carbon during the Palaeocene-Eocene Thermal Maximum. Nature 548, 573–577.

Gutjahr, M., Bordier, L., Douville, E., Farmer, J., Foster, G.L., Hathorne, E.C., Hönisch, B., Lemarchand, D., Louvat, P., McCulloch, M., Noireaux, J., Pallavicini, N., Rae, J.W.B., Rodushkin, I., Roux, P., Stewart, J.A., Thil, F., You, C.-F., 2020. Sub-Permil Interlaboratory Consistency for Solution-Based Boron Isotope Analyses on Marine Carbonates. Geostand. Geoanalytical Res. 45, 59–75.

Hain, M.P., Sigman, D.M., Higgins, J.A., Haug, G.H., 2015. The effects of secular calcium and magnesium concentration changes on the thermodynamics of seawater acid/base chemistry: implications for Eocene and Cretaceous ocean carbon chemistry and buffering. Glob. Biogeochem. Cycles 29, 517–533.

Hain, M.P., Sigman, D.M., Higgins, J.A., Haug, G.H., 2018. Response to Comment by Zeebe and Tyrrell on "The Effects of Secular Calcium and Magnesium Concentration Changes on the Thermodynamics of Seawater Acid/Base Chemistry: Implications for the Eocene and Cretaceous Ocean Carbon Chemistry and Buffering". Glob. Biogeochem. Cycles 32, 898–901.

Hansen, H.J., Buchardt, B., 1977. Depth distribution of *Amphistegina* in the Gulf of Eilat, Israel. Utrecht Micropaleont Bull 15, 205–224.

Harper, D.T., Hönisch, B., Zeebe, R.E., Shaffer, G., Haynes, L.L., Thomas, E., Zachos, J.C., 2020. The Magnitude of Surface Ocean Acidification and Carbon Release During Eocene Thermal Maximum 2 (ETM-2) and the Paleocene-Eocene Thermal Maximum (PETM). Paleoceanogr. Paleoclimatol. 35, e2019PA003699.

Hathorne, E.C., Gagnon, A., Felis, T., Adkins, J., Asami, R., Boer, W., Caillon, N., Case, D., Cobb, K.M., Douville, E., deMenocal, P., Eisenhauer, A., Garbe-Schönberg, D., Geibert, W., Goldstein, S., Hughen, K., Inoue, M., Kawahata, H., Kölling, M., Cornec, F.L., Linsley, B.K., McGregor, H.V., Montagna, P., Nurhati, I.S., Quinn, T.M., Raddatz, J., Rebaubier, H., Robinson, L., Sadekov, A., Sherrell, R., Sinclair, D., Tudhope, A.W., Wei, G., Wong, H., Wu, H.C., You, C.-F., 2013. Interlaboratory study

for coral Sr/Ca and other element/Ca ratio measurements. Geochem. Geophys. Geosystems 14, 3730–3750.
Hauzer, H., 2022. Development of new foraminiferal proxies for paleochemistry of the oceans. PhD thesis. The Hebrew University of Jerusalem.
Hauzer, H., Evans, D., Müller, W., Rosenthal, Y., Erez, J., 2018. Calibration of Na partitioning in the calcitic foraminifer *Operculina ammonoides* under variable Ca concentration: Toward reconstructing past seawater composition. Earth Planet. Sci. Lett. 497, 80–91.
Hauzer, H., Evans, D., Müller, W., Rosenthal, Y., Erez, J., 2021. Salinity Effect on Trace Element Incorporation in Cultured Shells of the Large Benthic Foraminifer *Operculina ammonoides*. Paleoceanogr. Paleoclimatology 36, e2021PA004218.
Haynes, L.L., Hönisch, B., Dyez, K.A., Holland, K., Rosenthal, Y., Fish, C.R., Subhas, A.V., Rae, J.W.B., 2017. Calibration of the B/Ca proxy in the planktic foraminifer *Orbulina universa* to Paleocene seawater conditions. Paleoceanography 32, 580–599.
Haynes, L.L., Hönisch, B., Holland, K., Rosenthal, Y., Eggins, S.M., 2019. Evaluating the planktic foraminiferal B/Ca proxy for application to deep time paleoceanography. Earth Planet. Sci. Lett. 528, 115824.
Heinrich, C.A., Pettke, T., Halter, W.E., Aigner-Torres, M., Audétat, A., Günther, D., Hattendorf, B., Bleiner, D., Guillong, M., Horn, I., 2003. Quantitative multi-element analysis of minerals, fluid and melt inclusions by laser-ablation inductively-coupled-plasma mass-spectrometry. Geochim. Cosmochim. Acta 67, 3473–3497.
Hemming, N.G., Hanson, G.N., 1992. Boron isotopic composition and concentration in modern marine carbonates. Geochim. Cosmochim. Acta 56, 537–543.
Henehan, M.J., Rae, J.W.B., Foster, G.L., Erez, J., Prentice, K.C., Kucera, M., Bostock, H. C., Martínez-Botí, M.A., Milton, J.A., Wilson, P.A., Marshall, B.J., Elliott, T., 2013. Calibration of the boron isotope proxy in the planktonic foraminifera *Globigerinoides ruber* for use in palaeo-CO_2 reconstruction. Earth Planet. Sci. Lett. 364, 111–122.
Henehan, M.J., Foster, G.L., Rae, J.W.B., Prentice, K.C., Erez, J., Bostock, H.C., Marshall, B.J., Wilson, P.A., 2015. Evaluating the utility of B/Ca ratios in planktic foraminifera as a proxy for the carbonate system: A case study of *Globigerinoides ruber*. Geochem. Geophys. Geosys. 16, 1052–1069.
Henehan, M.J., Foster, G.L., Bostock, H.C., Greenop, R., Marshall, B.J., Wilson, P.A., 2016. A new boron isotope-pH calibration for *Orbulina universa*, with implications for understanding and accounting for 'vital effects'. Earth Planet. Sci. Lett. 454, 282–292.
Henehan, M.J., Edgar, K.M., Foster, G.L., Penman, D.E., Hull, P.M., Greenop, R., Anagnostou, E., Pearson, P.N., 2020. Revisiting the Middle Eocene Climatic Optimum Carbon Cycle Conundrum With New Estimates of Atmospheric pCO_2 From Boron Isotopes. Paleoceanogr. Paleoclimatol. 35, e2019PA003713.
Henehan, M.J., Gebbinck, C.D.K., Wymans, J.V.B., Hain, M.P., Rae, J.W.B., Hönisch, B., Foster, G.L., Kim, S.-T., 2022. No ion is an island: Multiple ions influence boron incorporation into $CaCO_3$. Geochim. Cosmochim. Acta 318, 510–530.
Hohenegger, J., Yordanova, E., Nakano, Y., Tatzreiter, F., 1999. Habitats of larger foraminifera on the upper reef slope of Sesoko Island, Okinawa. Japan. *Mar. Micropaleontol.* 36, 109–168.
Holzmann, M., Hohenegger, J., Apothéloz-Perret-Gentil, L., Morard, R., Abramovich, S., Titelboim, D., Pawlowski, J., 2022. *Operculina* and *Neoassilina*: a revision of recent nummulitid genera based on molecular and morphological data reveals a new genus. J. Earth Sci. 33, 1411–1424.
Hönisch, B., Bijma, J., Russell, A.D., Spero, H.J., Palmer, M.R., Zeebe, R.E., Eisenhauer, A., 2003. The influence of symbiont photosynthesis on the boron isotopic composition of foraminifera shells. Mar. Micropaleontol. 49, 87–96.
Hönisch, B., Hemming, N.G., Archer, D., Siddall, M., McManus, J.F., 2009. Atmospheric carbon dioxide concentration across the mid-pleistocene transition. Science 324, 1551–1554.
Hönisch, B., Eggins, S.M., Haynes, L.L., Allen, K.A., Holland, K.D., Lorbacher, K., 2019. Boron Proxies in Paleoceanography and Paleoclimatology. Wiley-Blackwell.
Hottinger, L., 1977. Foraminifères Operculiniformes. PhD Thesis, Mém du Muséum Natl d'Histoire Nat.
Howes, E.L., Kaczmarek, K., Raitzsch, M., Mewes, A., Bijma, N., Horn, I., Misra, S., Gattuso, J.-P., Bijma, J., 2017. Decoupled carbonate chemistry controls on the incorporation of boron into *Orbulina universa*. Biogeosciences 14, 415–430.
Humphreys, M.P., Lewis, E.R., Sharp, J.D., Pierrot, D., 2022. PyCO2SYS v1. 8: Marine car bonate system calculations in Python. Geosci. Model Develop. 15 (1), 15–43.
Inglis, G.N., Bragg, F., Burls, N.J., Cramwinckel, M.J., Evans, D., Foster, G.L., Huber, M., Lunt, D.J., Siler, N., Steinig, S., Tierney, J.E., Wilkinson, R., Anagnostou, E., de Boer, A.M., Dunkley, J.T., Edgar, K.M., Hollis, C.J., Hutchinson, D.K., Pancost, R.D., 2020. Global mean surface temperature and climate sensitivity of the early Eocene Climatic Optimum (EECO), Paleocene-Eocene Thermal Maximum (PETM), and latest Paleocene. Clim. past 16, 1953–1968.
Jochum, K.P., Nohl, U., Herwig, K., Lammel, E., Stoll, B., Hofmann, A.W., 2005. GeoReM: a new geochemical database for reference materials and isotopic standards. Geostand. Geoanalytical Res. 29, 333–338.
Jochum, K.P., Weis, U., Stoll, B., Kuzmin, D., Yang, Q., Raczek, I., Jacob, D.E., Stracke, A., Birbaum, K., Frick, D.A., Günther, D., Enzweiler, J., 2011. Determination of reference values for NIST SRM 610–617 glasses following ISO guidelines. Geostand. Geoanalytical Res. 35, 397–429.
Jochum, K.P., Garbe-Schönberg, D., Veter, M., Stoll, B., Weis, U., Weber, M., Lugli, F., Jentzen, A., Schiebel, R., Wassenburg, J.A., Jacob, D.E., Haug, G.H., 2019. Nano-Powdered Calcium Carbonate Reference Materials: Significant Progress for Microanalysis? Geostand. Geoanalytical Res. 43, 595–609.
Jørgensen, B.B., Erez, J., Revsbech, P., Cohen, Y., 1985. Symbiotic photosynthesis in a planktonic foraminiferan, *Globigerinoides sacculifer* (Brady), studied with microelectrodes 1. Limnol. Oceanogr. 30, 1253–1267.
Jurikova, H., Liebetrau, V., Gutjahr, M., Rollion-Bard, C., Hu, M.Y., Krause, S., Henkel, D., Hiebenthal, C., Schmidt, M., Laudien, J., Eisenhauer, A., 2019. Boron isotope systematics of cultured brachiopods: response to acidification, vital effects and implications for palaeo-pH reconstruction. Geochim. Cosmochim. Acta 248, 370–386.
Kennett, J., Srinivasan, M., 1983. Neogene planktonic foraminifera, A phylogenetic Atlas. Hutchinson Ross, Stroudsburg, Pennsylvania. 265 pp.
Klochko, K., Kaufman, A.J., Yao, W., Byrne, R.H., Tossell, J.A., 2006. Experimental measurement of boron isotope fractionation in seawater. Earth Planet. Sci. Lett. 248, 276–285.
Klochko, K., Cody, G.D., Tossell, J.A., Dera, P., Kaufman, A.J., 2009. Re-evaluating boron speciation in biogenic calcite and aragonite using ^{11}B MAS NMR. Geochim. Cosmochim. Acta 73, 1890–1900.
Ko, Y.H., Shin, S.-H., Kim, S.-G., Park, M.-O., Seok, M.-W., Kim, M.-S., Lee, K., Kim, D., Park, G.-H., Kim, T.-W., 2024. Significant CO_2 emission in the shallow inshore waters of the southeastern Yellow Sea in 2020. Mar. Pollut. Bull. 201, 116262.
Köhler-Rink, S., Kühl, M., 2000. Microsensor studies of photosynthesis and respiration in larger symbiotic foraminifera. I The physico-chemical microenvironment of *Marginopora vertebralis*, *Amphistegina lobifera* and *Amphisorus hemprichii*. Mar. Biol. 137, 473–486.
Köhler-Rink, S., Kühl, M., 2005. The chemical microenvironment of the symbiotic planktonic foraminifer *Orbulina universa*. Mar. Biol. Res. 1, 68–78.
Lauvset, S.K., Gruber, N., 2014. Long-term trends in surface ocean pH in the North Atlantic. Mar. Chem. 162, 71–76.
Lee, K., Kim, T.-W., Byrne, R.H., Millero, F.J., Feely, R.A., Liu, Y.-M., 2010. The universal ratio of boron to chlorinity for the North Pacific and North Atlantic oceans. Geochim. Cosmochim. Acta 74, 1801–1811.
Levi, A., Müller, W., Erez, J., 2019. Intrashell Variability of Trace Elements in Benthic Foraminifera Grown Under High CO_2 Levels. Front. Earth Sci. 7, 247.
Lewis, E., Wallace, D.W.R., 1998. Program Developed for CO_2 System Calculations. Carbon Dioxide Information Analysis Center, Oak Ridge National Laboratory, U.S. Department of Energy, Oak Ridge, TN, USA.
Lin, L., Hu, Z., Yang, L., Zhang, W., Liu, Y., Gao, S., Hu, S., 2014. Determination of boron isotope compositions of geological materials by laser ablation MC-ICP-MS using newly designed high sensitivity skimmer and sample cones. Chem. Geol. 386, 22–30.
Lueker, T.J., Dickson, A.G., Keeling, C.D., 2000. Ocean pCO_2 calculated from dissolved inorganic carbon, alkalinity, and equations for K_1 and K_2: validation based on laboratory measurements of CO_2 in gas and seawater at equilibrium. Mar. Chem. 70, 105–119.
Martínez-Botí, M.A., Marino, G., Foster, G.L., Ziveri, P., Henehan, M.J., Rae, J.W.B., Mortyn, P.G., Vance, D., 2015. Boron isotope evidence for oceanic carbon dioxide leakage during the last deglaciation. Nature 518, 219–222.
Masson-Delmotte V., Zhai P., Pirani A., Connors S.L., Péan C., Berger S., Caud N., Chen Y., Goldfarb L., Gomis M. I., Huang M., Leitzell K., Lonnoy E., Matthews J.B.R., Maycock, T.K., Waterfield, T., Yelekçi O., Yu, R., Zhou, B., 2021. IPCC, 2021: Climate Change 2021: The Physical Basis. Contribution of Working Group I to the Sixth Assessment Report of the Intergovernmental Panel on Climate Change. Cambridge, United Kingdom and New York, NY, USA, pp. 33−144.
Mavromatis, V., Purgstaller, B., Louvat, P., Faure, L., Montouillout, V., Gaillardet, J., Schott, J., 2021. Boron isotope fractionation during the formation of amorphous calcium carbonates and their transformation to Mg-calcite and aragonite. Geochim. Cosmochim. Acta 315, 152–171.
McClelland, H.L.O., Halevy, I., Wolf-Gladrow, D.A., Evans, D., Bradley, A.S., 2021. Statistical uncertainty in paleoclimate proxy reconstructions. Geophys. Res. Lett. 48, e2021GL092773.
McCulloch, M.T., D'Olivo, J.P., Falter, J., Holcomb, M., Trotter, J.A., 2017. Coral calcification in a changing World and the interactive dynamics of pH and DIC upregulation. Nat. Commun. 8, 15686.
Millero, F.J., 2005. Chemical oceanography, third ed. CRC Press.
Müller, W., Shelley, M., Miller, P., Broude, S., 2009. Initial performance metrics of a new custom-designed ArF excimer LA-ICPMS system coupled to a two-volume laser-ablation cell. J Anal Spectrom 24, 209–214.
Nambiar, R., Hauzer, H., Gray, W.R., Henehan, M.J., Cotton, L., Erez, J., Rosenthal, Y., Renema, W., Müller, W., Evans, D., 2023. Controls on potassium incorporation in foraminifera and other marine calcifying organisms. Geochim. Cosmochim. Acta 351, 125–138.
Nir, O., Vengosh, A., Harkness, J.S., Dwyer, G.S., Lahav, O., 2015. Direct measurement of the boron isotope fractionation factor: reducing the uncertainty in reconstructing ocean paleo-pH. Earth Planet. Sci. Lett. 414, 1–5.
Noireaux, J., Mavromatis, V., Gaillardet, J., Schott, J., Montouillout, V., Louvat, P., Rollion-Bard, C., Neuville, D.R., 2015. Crystallographic control on the boron isotope paleo-pH proxy. Earth Planet. Sci. Lett. 430, 398–407.
Oron, S., Abramovich, S., Almogi-Labin, A., Woeger, J., Erez, J., 2018. Depth related adaptations in symbiont bearing benthic foraminifera: New insights from a field experiment on *Operculina ammonoides*. Sci. Rep. 8, 9560.
Oron, S., Evans, D., Abramovich, S., Almogi-Labin, A., Erez, J., 2020. Differential sensitivity of a symbiont-bearing foraminifer to seawater carbonate chemistry in a decoupled DIC-pH experiment. J. Geophys. Res. Biogeosciences 125, e2020JG005726.
Orr, J.C., Epitalon, J.-M., Dickson, A.G., Gattuso, J.-P., 2018. Routine uncertainty propagation for the marine carbon dioxide system. Mar. Chem. 207, 84–107.
Palaeosens, 2012. Making sense of palaeoclimate sensitivity. Nature 491, 683–691.
Parkhurst, D.L., Appelo, C.A.J., 2013). PHREEQC version 3: a computer program for speciation, batch-reaction, one-dimensional transport, and inverse geochemical calculations.
Pokrovski, G.S., Schott, J., Sergeyev, A.S., 1995. Experimental determination of the stability constants of $NaSO_4^-$ and $NaB(OH)_4^0$ in hydrothermal solutions using a new

high-temperature sodium-selective glass electrode — Implications for boron isotopic fractionation. Chem. Geol. 124, 253–265.
Rae, J.W.B., 2018. Boron Isotopes in Foraminifera: Systematics, Biomineralisation, and CO_2 Reconstruction. In: *Boron Isotopes* Advances in Isotope Geochemistry. Springer, pp. 107–143.
Rae, J.W.B., Foster, G.L., Schmidt, D.N., Elliott, T., 2011. Boron isotopes and B/Ca in benthic foraminifera: Proxies for the deep ocean carbonate system. Earth Planet. Sci. Lett. 302, 403–413.
Rae, J.W.B., Zhang, Y.G., Liu, X., Foster, G.L., Stoll, H.M., Whiteford, R.D.M., 2021. Atmospheric CO_2 over the Past 66 Million Years from Marine Archives. Annu. Rev. Earth Planet. Sci. 49, 599–631.
Raimondi, L., Matthews, J.B.R., Atamanchuk, D., Azetsu-Scott, K., Wallace, D.W.R., 2019. The internal consistency of the marine carbon dioxide system for high latitude shipboard and in situ monitoring. Mar. Chem. 213, 49–70.
Renema, W., 2002. Larger foraminifera as marine environmental indicators. Scr. Geol. 124, 1–260.
Renema, W., Beaman, R.J., Webster, J.M., 2013. Mixing of relict and modern tests of larger benthic foraminifera on the Great Barrier Reef shelf margin. Mar. Micropaleontol. 101, 68–75.
Renema, W., Troelstra, S.R., 2001. Larger foraminifera distribution on a mesotrophic carbonate shelf in SW Sulawesi (Indonesia). Palaeogeogr. Palaeoclimatol. Palaeoecol. 175, 125–146.
Ridgwell, A., 2005. A Mid Mesozoic Revolution in the regulation of ocean chemistry. Mar. Geol. 217, 339–357.
Rink, S., Kühl, M., Bijma, J., Spero, H.J., 1998. Microsensor studies of photosynthesis and respiration in the symbiotic foraminifer *Orbulina universa*. Mar. Biol. 131, 583–595.
Rollion-Bard, C., Erez, J., 2010. Intra-shell boron isotope ratios in the symbiont-bearing benthic foraminiferan *Amphistegina lobifera*: Implications for $\delta^{11}B$ vital effects and paleo-pH reconstructions. Geochim. Cosmochim. Acta 74, 1530–1536.
Rosman, K.J.R., Taylor, P.D.P., 1997. Isotopic composition of the element.
Sadekov, A., Lloyd, N.S., Misra, S., Trotter, J., D'Olivo, J., McCulloch, M., 2019. Accurate and precise microscale measurements of boron isotope ratios in calcium carbonates using laser ablation multicollector-ICPMS. J. Anal. at. Spectrom. 34, 550–560.
Sanyal, A., Hemming, N.G., Hanson, G.N., Broecker, W.S., 1995. Evidence for a higher pH in the glacial ocean from boron isotopes in foraminifera. Nature 373, 234–236.
Sanyal, A., Hemming, N.G., Broecker, W.S., Lea, D.W., Spero, H.J., Hanson, G.N., 1996. Oceanic pH control on the boron isotopic composition of foraminifera: evidence from culture experiments. Paleoceanography 11, 513–517.
Sanyal, A., Bijma, J., Spero, H., Lea, D.W., 2001. Empirical relationship between pH and the boron isotopic composition of *Globigerinoides sacculifer* : Implications for the boron isotope paleo-pH proxy. Paleoceanography 16, 515–519.
Segev, E., Erez, J., 2006. Effect of Mg/Ca ratio in seawater on shell composition in shallow benthic foraminifera. Geochem. Geophys. Geosystems 7, Q02P09.
Shaw, E.C., McNeil, B.I., 2014. Seasonal variability in carbonate chemistry and air–sea CO_2 fluxes in the southern Great Barrier Reef. Mar. Chem. 158, 49–58.
Spezzaferri, S., Coxall, H.K., Olsson, R.K., Hemleben, C., 2018. Taxonomy, biostratigraphy, and phylogeny of Oligocene *Globigerina*, *Globigerinella*, and *Quiltyella* N. Gen. Cushman Found. Foraminifer. Res. 179–214.
Standish, C.D., Chalk, T.B., Babila, T.L., Milton, J.A., Palmer, M.R., Foster, G.L., 2019. The effect of matrix interferences on in situ boron isotope analysis by laser ablation multi-collector inductively coupled plasma mass spectrometry. Rapid Commun. Mass Spectrom. 33, 959–968.
Stewart, J.A., Christopher, S.J., Kucklick, J.R., Bordier, L., Chalk, T.B., Dapoigny, A., Douville, E., Foster, G.L., Gray, W.R., Greenop, R., Gutjahr, M., Hemsing, F., Henehan, M.J., Holdship, P., Hsieh, Y., Kolevica, A., Lin, Y., Mawbey, E.M., Rae, J. W.B., Robinson, L.F., Shuttleworth, R., You, C., Zhang, S., Day, R.D., 2021. NIST RM 8301 Boron Isotopes in Marine Carbonate (Simulated Coral and Foraminifera Solutions): Inter-laboratory $\delta^{11}B$ and Trace Element Ratio Value Assignment. Geostand. Geoanalytical Res. 45, 77–96.
Takahashi, T., Sutherland, S.C., Wanninkhof, R., Sweeney, C., Feely, R.A., Chipman, D. W., Hales, B., Friederich, G., Chavez, F., Sabine, C., Watson, A., Bakker, D.C.E., Schuster, U., Metzl, N., Yoshikawa-Inoue, H., Ishii, M., Midorikawa, T., Nojiri, Y., Körtzinger, A., Steinhoff, T., Hoppema, M., Olafsson, J., Arnarson, T.S., Tilbrook, B., Johannessen, T., Olsen, A., Bellerby, R., Wong, C.S., Delille, B., Bates, N.R., de Baar, H.J.W., 2009. Climatological mean and decadal change in surface ocean pCO_2, and net sea–air CO_2 flux over the global oceans. *Deep Sea Res.* Part II Top. Stud. Oceanogr. 56, 554–577.
ter Kuile, B., Erez, J., 1987. Uptake of inorganic carbon and internal carbon cycling in symbiont-bearing benthonic foraminifera. Mar. Biol. 94, 499–509.
Terlouw, G.J., Knor, L.A.C.M., De Carlo, E.H., Drupp, P.S., Mackenzie, F.T., Li, Y.H., Sutton, A.J., Plueddemann, A.J., Sabine, C.L., 2019. Hawaii Coastal Seawater CO_2 network: a statistical evaluation of a decade of observations on tropical coral reefs. Front. Mar. Sci. 6, 226.
Tierney, J.E., Zhu, J., King, J., Malevich, S.B., Hakim, G.J., Poulsen, C.J., 2020. Glacial cooling and climate sensitivity revisited. Nature 584, 569–573.
Toyofuku, T., Matsuo, M.Y., de Nooijer, L.J., Nagai, Y., Kawada, S., Fujita, K., Reichart, G.-J., Nomaki, H., Tsuchiya, M., Sakaguchi, H., Kitazato, H., 2017. Proton pumping accompanies calcification in foraminifera. Nat. Commun. 8, 14145.
Trotter, J., Montagna, P., McCulloch, M., Silenzi, S., Reynaud, S., Mortimer, G., Martin, S., Ferrier-Pagès, C., Gattuso, J.-P., Rodolfo-Metalpa, R., 2011. Quantifying the pH 'vital effect' in the temperate zooxanthellate coral *Cladocora caespitosa*: Validation of the boron seawater pH proxy. Earth Planet. Sci. Lett. 303, 163–173.
Van Dijk, I., De Nooijer, L.J., Reichart, G.-J., 2017. Trends in element incorporation in hyaline and porcelaneous foraminifera as a function of pCO_2. Biogeosciences 14, 497–510.
Virtanen, P., Gommers, R., Oliphant, T.E., Haberland, M., Reddy, T., Cournapeau, D., Burovski, E., Peterson, P., Weckesser, W., Bright, J., van der Walt, S.J., Brett, M., Wilson, J., Millman, K.J., Mayorov, N., Nelson, A.R.J., Jones, E., Kern, R., Larson, E., Carey, C.J., Polat, İ., Feng, Y., Moore, E.W., VanderPlas, J., Laxalde, D., Perktold, J., Cimrman, R., Henriksen, I., Quintero, E.A., Harris, C.R., Archibald, A.M., Ribeiro, A. H., Pedregosa, F., van Mulbregt, P., SciPy 1.0 Contributors, 2020. SciPy 1.0: Fundamental Algorithms for Scientific Computing in Python. Nat. Methods 17, 261–272.
Westerhold, T., Marwan, N., Drury, A.J., Liebrand, D., Agnini, C., Anagnostou, E., Barnet, J.S.K., Bohaty, S.M., Vleeschouwer, D.D., Florindo, F., Frederichs, T., Hodell, D.A., Holbourn, A.E., Kroon, D., Lauretano, V., Littler, K., Lourens, L.J., Lyle, M., Pälike, H., Röhl, U., Tian, J., Wilkens, R.H., Wilson, P.A., Zachos, J.C., 2020. An astronomically dated record of Earth's climate and its predictability over the last 66 million years. Science 369, 1383–1387.
Williams, N.L., Juranek, L.W., Feely, R.A., Johnson, K.S., Sarmiento, J.L., Talley, L.D., Dickson, A.G., Gray, A.R., Wanninkhof, R., Russell, J.L., Riser, S.C., Takeshita, Y., 2017. Calculating surface ocean pCO_2 from biogeochemical Argo floats equipped with pH: An uncertainty analysis: Calculating Ocean pCO_2 From Float pH. Glob. Biogeochem. Cycles 31, 591–604.
Wolf-Gladrow, D.A., Bijma, J., Zeebe, R.E., 1999. Model simulation of the carbonate chemistry in the microenvironment of symbiont bearing foraminifera. Mar. Chem. 64, 181–198.
Yan, H., Yu, K., Shi, Q., Lin, Z., Zhao, M., Tao, S., Liu, G., Zhang, H., 2018. Air-sea CO_2 fluxes and spatial distribution of seawater pCO_2 in Yongle Atoll, northern-central South China Sea. Cont. Shelf Res. 165, 71–77.
Yu, J., Elderfield, H., 2007. Benthic foraminiferal B/Ca ratios reflect deep water carbonate saturation state. Earth Planet. Sci. Lett. 258, 73–86.
Yu, J., Elderfield, H., Hönisch, B., 2007. B/Ca in planktonic foraminifera as a proxy for surface seawater pH. Paleoceanography 22, PA2202.
Yu, J., Thornalley, D.J.R., Rae, J.W.B., McCave, N.I., 2013. Calibration and application of B/Ca, Cd/Ca, and $\delta^{11}B$ in *Neogloboquadrina pachyderma* (sinistral) to constrain CO_2 uptake in the subpolar North Atlantic during the last deglaciation. Paleoceanography 28, 237–252.
Zachos, J.C., Dickens, G.R., Zeebe, R.E., 2008. An early Cenozoic perspective on greenhouse warming and carbon-cycle dynamics. Nature 451, 279–283.
Zeebe, R.E., Rae, J.W.B., 2020. Equilibria, kinetics, and boron isotope partitioning in the aqueous boric acid–hydrofluoric acid system. Chem. Geol. 550, 119693.
Zeebe, R.E., Tyrrell, T., 2019. History of carbonate ion concentration over the last 100 million years II: Revised calculations and new data. Geochim. Cosmochim. Acta 257, 373–392.
Zeebe, R.E., Wolf-Gladrow, D., 2001. CO_2 in seawater: equilibrium, kinetics, isotopes. Gulf Professional Publishing.
Zeebe, R.E., Wolf-Gladrow, D.A., Bijma, J., Hönisch, B., 2003. Vital effects in foraminifera do not compromise the use of $\delta^{11}B$ as a paleo-pH indicator: Evidence from modeling. Paleoceanography 18, 1043.